



# Biomedical Imaging: Principles, Technologies, Clinical Aspects, Contrast Agents, Limitations and Future Trends in Nanomedicines

Justine Wallyn<sup>1</sup> · Nicolas Anton<sup>1</sup> · Salman Akram<sup>1</sup> · Thierry F. Vandamme<sup>1</sup>

Received: 14 November 2018 / Accepted: 11 March 2019 / Published online: 3 April 2019  
© Springer Science+Business Media, LLC, part of Springer Nature 2019

**ABSTRACT** This review article presents the state-of-the-art in the major imaging modalities supplying relevant information on patient health by real-time monitoring to establish an accurate diagnosis and potential treatment plan. We draw a comprehensive comparison between all imagers and ultimately end with our focus on two main types of scanners: X-ray CT and MRI scanners. Numerous types of imaging probes for both imaging techniques are described, as well as reviewing their strengths and limitations, thereby showing the current need for the development of new diagnostic contrast agents (CAs). The role of nanoparticles in the design of CAs is then extensively detailed, reviewed and discussed. We show how nanoparticulate agents should be promising alternatives to molecular ones and how they are already paving new routes in the field of nanomedicine.

**KEYWORDS** contrast agent · magnetic resonance imaging · medical imaging · nanomedicine · x-ray imaging

## ABBREVIATIONS

2D	2-Dimension
3D	3-Dimension
API	Active principle ingredient
CA	Contrast agent
CNS	Central nervous system
CT	Computed tomography
DDS	Drug delivery system

DEs	Dendrimers
EPR	Enhanced permeability and retention
FDA	Food and drug administration
GI	Gastrointestinal
HDL	High-density lipoprotein
HU	Hounsfield unit
IONPs	Iron oxide nanoparticles
LDL	Low-density lipoprotein
LPs	Liposomes
LPPs	Lipoproteins
NCs	Nanocarriers
NMR	Nuclear magnetic resonance
NPs	Nanoparticles
MRI	Magnetic resonance imaging
PAMAM	Poly(Amidoamine)
PCL	Poly( $\epsilon$ -Caprolactone)
PEG	Poly(Ethylene Glycol)
PLA	Poly(Lactic Acid)
PLGA	Poly(Lactic-co-Glycolic Acid)
PET	Positron emission tomography
PO	Poly(Propylene Oxide)
RES	Reticuloendothelial system
ROI	Region of interest
SPECT	Single-photon emission computed tomography
SPIONs	Superparamagnetic iron oxide nanoparticles
USPIOs	Ultrasmall superparamagnetic iron oxide
VLDL	Very low-density lipoprotein

## NONINVASIVE IMAGING MODALITIES: FROM PRINCIPLES TO PREVALENT TECHNIQUES

### Diagnostic by Imaging Techniques

The noninvasive diagnostic field has seen outstanding progress due to the development of advanced imagers. Owing to computing power growth, current imaging techniques aim at

✉ Nicolas Anton  
nanton@unistra.fr

<sup>1</sup> Université de Strasbourg, CNRS, CAMB UMR 7199  
F-67000 Strasbourg, France

providing complete visualization from the molecular scale to cellular, organ, tissue, lesion scales and to the whole organism scale. An arsenal of tools dedicated to imaging has emerged over several decades and currently allows us to understand and examine the medical profile of patients by acquiring reconstructed 2D or 3D images without invasive monitoring in patients. Because of the difference in contrast from one region to another, images show clear delineation of internal structure (anatomy), morphology, and physiological functions at the different aforementioned scales. Consequently, engineered images provide a basis for the detection of early-stage pathology, evaluation of the progression of diseases, cancer staging, treatment efficacy follow-up, etc. and assist in clinical decision making for patient disease management. Improved and fast screening by imaging has become the most essential and efficient noninvasive method to reduce patient mortality caused by a lack of reliable information about *in vivo* systems. To increase the visibility of the internal body structure by changing the contrast between healthy and unhealthy areas, exogenous pharmaceutical contrast enhancers, which are also called contrast agents (CA) or traceable probes, can be administered to patients to increase the sensitivity and/or specificity of a modality to a targeted region of interest (ROI) [1–5].

In this way, all imaging techniques provide precious information at their own scale and limits. The choice of modality is dictated by the type of data that we want to obtain from our technique (such as *in vivo* phenomena, i.e., functional processes or biochemical mechanisms, or biological entities and tissues, e.g., cells, stem cells, pathological tissues). Analyzing imaging techniques via a step-by-step approach is an appropriate way to develop an efficient and relevant diagnostic process [6]. Figure 1 displays basic and schematic methodology towards this goal.

In summary, diagnostic methodology relies on some key steps:

1. Define the scale level that must be precisely observed
2. Find suitable probes.
3. Find imaging instrumentation(s) sufficiently capable of imaging the target.
4. Check patient sensitivity to component-based probes
5. Conduct a small-scale study in preclinical research to optimize not only the acquisition process but also the CA composition and formulation (this additional step is required only if there are no previous data available that establish the clinical safety of the process).
6. Perform imaging when translation to the human scale is developed and reliable.

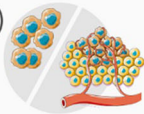




## Overview and Comparison of Imaging Instruments

There are five prime imaging techniques dedicated for preclinical and clinical biomedical applications. The most

commonly used imaging modalities are X-ray computed tomography (X-ray CT); magnetic resonance imaging (MRI); optical imaging by fluorescence and bioluminescence; nuclear imaging, including positron emission tomography (PET) and single-photon emission computed tomography (SPECT); and ultrasound imaging. The existence of such a wide range of imaging techniques is mainly due to their respective abilities to reveal structural and/or functional information at different scales and accuracy levels. All modalities rely on their own principle and therefore possess their own strengths and disadvantages regarding their resolution, sensitivity, depth of tissue penetration and contrast quantification. Because of their inherent principle, each imager requires its own kind of probe to yield efficient diagnosis and to highlight some poorly contrasted tissues [1–5]. Most features of these imagers are collected in Table 1.

To take full advantage of the main benefits of each imaging modality, instrumental limitations and interactions among the source, body tissues and fluids and probes must also be considered to identify the most suitable technique for tracking a specific *in vivo* target, as mentioned before [1, 5, 7]. The accuracy of diagnosis through noninvasive imaging tools relies on the quality of images and the amount of details that can be extracted from acquired pictures. Therefore, high resolution is desired even if CAs are used. Considering data from Table 1, it clearly appears that imagers based on ultrasound technology, PET and SPECT are lacking in this regard. Furthermore, PET and SPECT involve radioactive material, provide only physiological information and are not reliable for *in vivo* locations, rendering those two techniques inadequate [8]. Usually, physicians prefer what it is commonly called a cold modality for which no radiative probes are administered, or they combine nuclear imaging with a complementary imaging technique. Ultrasound imaging has recently seen tremendous evolution due to the progress of computed 3D reconstruction and palliation of motion artifacts. Ultrasound techniques, which are typically applied in clinical research in obstetrics, cardiology, surgery guidance and urology, have many advantages. However, ultrasound techniques are not efficient when we need to observe subtle details of the anatomy of deep tissue. Despite this, promising outcomes in molecular imaging have made ultrasound imaging increasingly interesting [9, 10]. Concerning optical imaging, this method is basically employed in combination with fluorophores such as organic dyes and inorganic nanoprobe such as quantum dots for molecular and cellular imaging, sensing, drug delivery, and targeting [11–13]. Optical imaging involves the use of luminescent or fluorescent reporter genes or parenteral administration of fluorescent or luminescent probes. The current status of this imaging modality, unlike the CT/MRI modality, is that it is used for only preclinical studies; however, clinical

**Fig. 1** Step-by-step guide to perform a diagnostic procedure by noninvasive imaging.

1	 <p>Biological mechanism Cells Organs</p>	<p><b>Identification of the target of investigation</b> <i>Biochemical process, cellular entity, zone of interest, pathology, whole body</i></p>
2	 <p>Commercial probe or need to prepare specific and new contrast agent</p>	<p><b>How to track the desired target?</b> <i>Use of probe(s) (there should be no interaction between probes to avoid harmful side effects on patient and loss of imaging efficiency). Direct or indirect visualization of the phenomena / zone of interest, suitable probe available for human application</i></p>
3	 <p>Resolution, depth of penetration <i>in vivo</i> information needed Availability in clinics</p>	<p><b>Selection of imaging modalities</b> <i>Unimodal or multimodal techniques, risk(s) for patient health, sensitivity to probe(s), convenient for clear visualization of target</i></p>
4	 <p>Preclinical imaging procedure on mice</p>	<p><b>Is preclinical trial on small animals necessary?</b> <i>Evaluation of the rarity of the case (well-known pathology or clinical trial), translation/scale-up of the imaging protocol already done to human</i></p>
5	 <p>Clinical imaging procedure on patient reconstruction of 2D or 3D images</p>	<p><b>Processing: administration of probe(s) and image acquisition</b> <i>Administration to adapted and specific exogenous contrasting substances to the target, survey of potential adverse effect on patient (allergy, intolerance, compatibility with treatment), engineering of images</i></p>

translation of optical imaging is under evaluation [14]. The clinical translation of optical imaging techniques is particularly supported by the cost and operating ease of optical

imaging instruments and the increasing number of probes, which are constantly in development [15–17]. Optical imaging has recently found important applications in the field

**Table 1** Comparison of the Most Common Clinical Imaging Techniques [1, 2, 4, 5, 7]

	X-ray CT	MRI	PET/SPECT	Ultrasound	Optical*
Source	X-ray	Magnetic field and radiofrequency	$\gamma$ -rays	Sound	Light
Spatial resolution	50–200 $\mu\text{m}$	25–100 $\mu\text{m}$	2–10 mm	50–500 $\mu\text{m}$	1–5 mm
Penetration depth	No limit***	No limit***	No limit***	Several cm	1–10 cm (depending of the technology used)
Probes	Heavy element, e.g., I, Ba, Au...	Magnetizable materials: $\text{Fe}_3\text{O}_4$ , Gd chelates	Radionuclide: $^{18}\text{F}$ , $^{11}\text{C}$ , $^{13}\text{N}$ , $^{15}\text{O}$ , $^{64}\text{Cu}$ , $^{124}\text{I}$ , $^{111}\text{In}$ , $^{99\text{m}}\text{Tc}$	Microbubble, emulsion, micelle	Fluorescent dye, quantum dots, near-infrared dyes
Probe dose (mol/L)	$10^{-3}$	$10^{-3}$ – $10^{-5}$	$10^{-10}$ – $10^{-12}$	Not characterized	Biolum: $10^{-15}$ – $10^{-17}$ Fluor: $10^{-9}$ – $10^{-12}$
Information**	A and P	A, P and F	A, P and F	A and P	P and M
Advantages	High resolution, no depth limit	High spatial resolution, no radiation, no depth limit	High sensitivity to probes	Easy, fast, no ionizing radiation, cost-effective	Multichannel imaging, no radiation, sensitive to probe dose
Drawbacks	Radiation, poor soft tissue delineation, low sensitivity to probes	Poor sensitivity to probes, expensive	Need for probes, radiation, expensive, low resolution	Depth limit (cm), poor contrast, not suitable for air-containing organs	Need for probes, not yet available in clinics, low depth penetration, low resolution

\*Optical imaging includes bioluminescence (biolum) and fluorescence (fluor) modalities

\*\*In vivo information: A: anatomical, P: physiological, F: functional and M: molecular

\*\*\*At the scales involved in clinical and preclinical studies

of early diagnosis, treatment of premalignancies, and real-time in vivo detection of surgical margins [18, 19]. In application to the detection of head and neck tumors, recent advances in optical hardware and reagents have provided unique opportunities for real-time premalignancy and cancer imaging in the clinic or operating room. A recent review on the main tools for this modality [18] described optical tools for these early detections, such as the use of autofluorescence imaging, targeted fluorescence imaging, high-resolution microendoscopy, narrow band imaging and Raman spectroscopy. The last two methods are the X-ray CT scanner and the MRI. The X-ray CT scanner is the oldest imager and involves an ionizing beam, but it remains one of the most commonly used techniques in clinics due to its cost-effectiveness, the quantitative information depicted on its scans, and its fast image acquisition and processing. However, compared to the non-radiation-based MRI technique, X-ray CT is not as efficient in contrasting soft tissues but still constitutes an alternative to patients who bear magnetizable devices (e.g., a specific prosthesis) [7, 20].

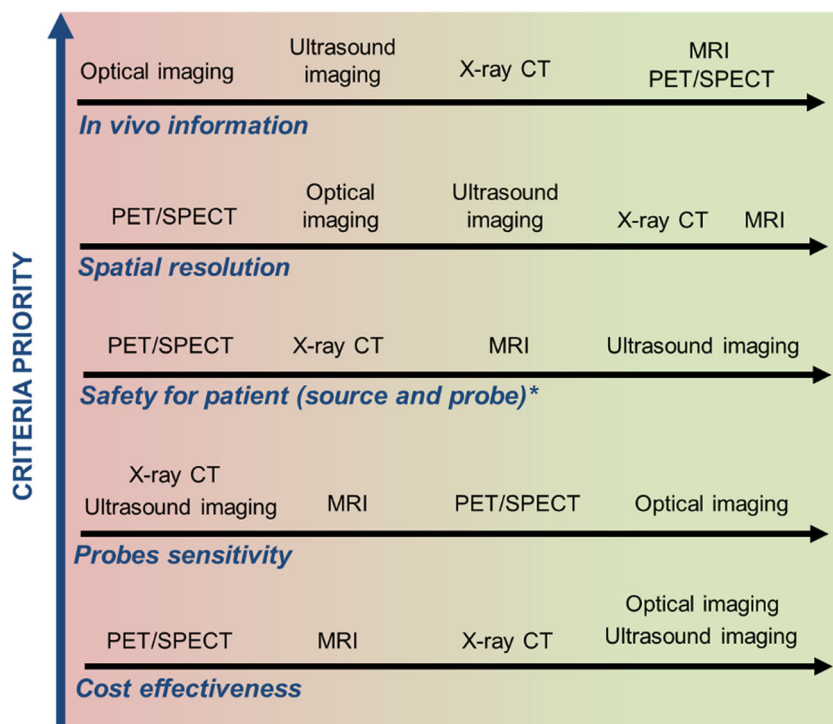
Using features from Table I, classification of imagers based on their cost, the dose of CA required to obtain contrast enhancement, the impact of the source, the toxicity of the probe, the spatial resolution needed for accurate reconstruction of an ROI and the in vivo information provided is introduced in Fig. 2. Criteria were classified from the relatively less (bottom) to the most (top) important point to focus on when establishing a diagnostic. Comparing each modality along with each criterion clearly

demonstrates that compared to clinical modalities, MRI and X-ray CT perform better, typically due to the collection of meaningful data from their high-resolution scans. It also appears that they are not as sensitive to probes as PET and SPECT, although radiopaque CAs and magnetic formulations are safer. Furthermore, neither of them have a depth penetration limit, meaning that organisms may be completely scoped.

According to the above figure, MRI and X-ray scanners are currently widely used and highly efficient imaging instruments. Progress in preclinical research has made them highly accessible and thus enhanced their use in clinical settings. However, there is no general consensus regarding which technique will be used for a specific disease. However, in many studies, MRI and X-ray scanners were selected as instruments or complementary devices for each other with the highest efficiency to perform a diagnosis free of ambiguous information, such as in cases of abdominal imaging (soft tissues) [21], hepatic lesions [22, 23], real masses [24] and pancreatic cancer [25, 26].

The next section will summarize the basic principles of X-ray CT and MRI. Their main characteristics and corresponding CAs will be introduced, and their advantages and drawbacks will be outlined to provide a comprehensive overview. We will explain why these two clinical scanners have become outstanding technologies as diagnostic tools for imaging investigations.

**Fig. 2** Classification of imaging modalities based on Table I.



\* Optical imaging is not included in this category because such modality is still not available for human translation.

## X-RAY SCANNER

### From X-Ray Discovery to X-Ray Imagers

The application of X-rays for biomedical imaging was recognized soon after the discovery of X-rays by W.C. Röntgen, a German physicist, in 1895. The curiosity and passion of Röntgen for this unknown kind of rays led him to write “On a new kind of rays” [27]. In this book, he described in 17 points his observations on what he finally named “X-rays” since no one had previously reported this kind of ray. Although understanding X-ray phenomena was laborious, it appeared as a substantial breakthrough in physics, and many applications of these rays developed in a very short time. Several decades later, during the 1960s, the development of X-rays for visualization of the inside of living organisms became very promising and drove A.M. Cormack and G.N. Hounsfield to create the first X-ray imagers for biomedical imaging purposes. The first computer-assisted X-ray tomography prototype was thus set up in clinics in 1972. A.M. Cormack and G.N. Hounsfield shared the Nobel Prize in Physiology or Medicine in 1979 for this tremendous innovation for preclinical research and medicine [28–33].

### Radiography: Principle and Instruments

An X-ray imager furnishes images on which tissues can be identified by exhibiting differences of opacification because their ability to attenuate X-rays by absorption of a part of their energy. The scanner and contrasting process works as illustrated in Fig. 3 and as follows: i) X-rays have to be generated and ii) pass through the specimen. The production of X-ray photons is carried out by an electron beam generated by high voltage, accelerated within a vacuum chamber and guided towards a heavy metal anode. iii) The resulting electromagnetic radiation then penetrates into the specimen. Depending on the nature of molecules *in vivo*, iv) interaction with X-ray photons may occur and may lead to absorption, reflection, or scattering of the incident X-ray photon. X-ray attenuation follows the Beer-Lambert exponential attenuation law and is multifactorial-dependent because it can be promoted by the electron density and the absorption coefficient of the element present within the *in vivo* media, the energy of the X-ray photon, the thickness of the subject, etc. Then, v) the total attenuation produced by the body is measured by detection of the emergent X-ray beam. Opacification of tissues can then be visualized on tomographic 2D images, i.e., sectional images reconstructed by an algorithm, and volumetric 3D reconstruction can be performed by stacking transverse sections. Contrast is measured by means of a grayscale. Dense materials absorb significant amounts of X-ray energy and lead to whitening of the image (from white to light gray). Water, in contrast, is not able to attenuate such photons; as a result, fluids

appear dark (from dark gray to black). Other tissues, such as soft tissues, are mostly contrasted by gray shades.

Quantification of opacification is performed using the Hounsfield unit (HU) calibrated with water. Using the Hounsfield scale, water and air are attributed values of 0 HU and  $-1000$  HU, respectively. Soft tissues are generally approximately  $-100$  HU to  $+100$  HU. Attenuation values of mineralized materials, such as skeletons, vary from  $+400$  to  $+1000$  HU ( $-1000$  HU for air-containing organs such as lungs). Based on this scale, the attenuation value for a target of interest is determined according to Eq. 1 [1, 2, 20, 29, 30, 32, 34]:

$$HU = 1000 \times \left( \frac{\mu - \mu_{\text{water}}}{\mu_{\text{water}}} \right) \quad (1)$$

where  $\mu$  and  $\mu_{\text{water}}$  are the linear X-ray attenuation coefficient of the target of interest and water, respectively.

Radiography is a general term that includes all types of X-ray scanners. The clinical device is known as X-ray computed tomography (i.e., X-ray CT), whereas the preclinical prototype instrument, dedicated to small animal studies in the research laboratory, is microcomputed tomography (i.e., micro-CT). Those two scanners differ in their resolution. Indeed, investigation on small laboratory subjects requires tools allowing us to examine at an equivalent scale equivalence and thus with higher spatial and temporal resolution. Nevertheless, micro-CT is simply inaccurately used as a broad term to refer to a group of three X-ray microscopic scanners with specific spatial resolutions: mini-CT ( $50$ – $200$   $\mu\text{m}$ ), micro-CT ( $1$ – $50$   $\mu\text{m}$ ) and nano-CT ( $0.1$ – $1$   $\mu\text{m}$ ) (Fig. 4). Commonly, preclinical imaging research uses micro-CT to conduct small-scale investigations on small laboratory animals such as mice [34–38].

The potential of X-ray scanners is determined by conducting a benefit-to risk assessment of these instruments. Although there are many advantages of this technique, the main limitation of such a device is the delivery of a high radiation dose, which causes long-term genetic damage. Even though the radiation dose is adjusted to the desired *in vivo* target, radiation may induce cancer and/or increase cancer lifetime. One study showed that [39] the radiation impact was multifactorial and that damage by radiation depends on the number of scans, photon energy, number of X-ray sources, closeness of the specimen to the source(s), and scan speed applied. All these factors are adjusted according to the size of the region imaged and the type of specimen. Nevertheless, the damage can be minimized if physicians agree to compromise the quality of the image to prevent acute tissue damage and patient health. Because of the potential damage, the parameters can be adjusted for repeated diagnosis [2, 38–40].

Despite the radiation issue, X-ray scanners remain an important tool for clinics since they are cost-effective, fast, and high resolution and have no depth limits. However, early

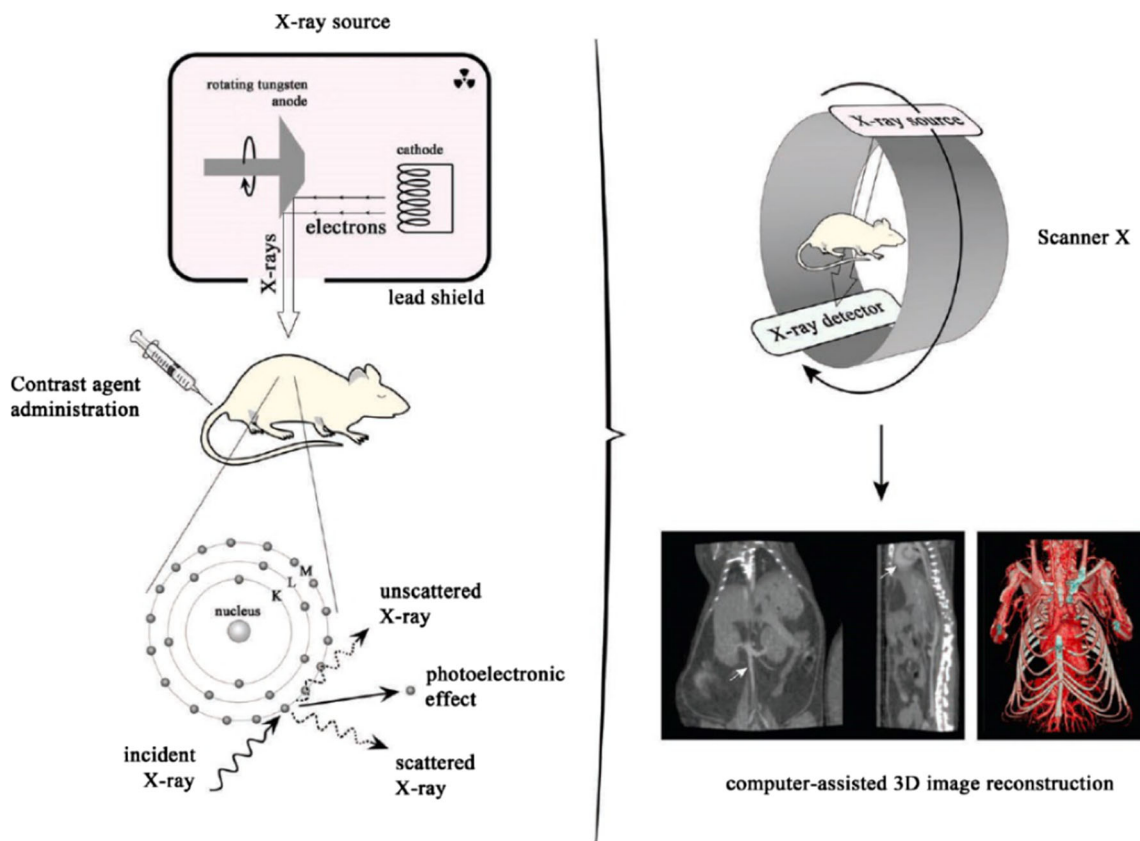


**Fig. 3** Schematic representation of the X-ray scanner principle and typical 3D reconstructed images obtained by an X-ray imaging protocol (reproduced with permission from [31]).

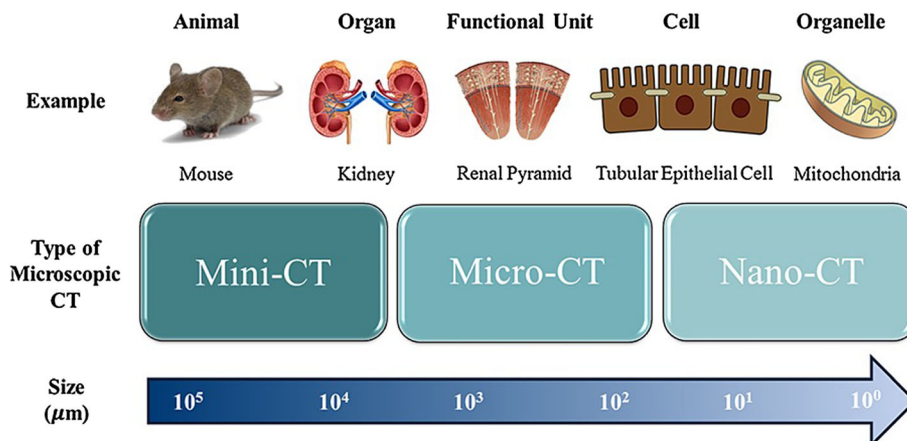
diagnosis of soft-tissue pathology can be challenging due to a lack of clear delineation between soft tissues. Indeed, very subtle changes in their X-ray attenuation are observed on CT scans, making it difficult to identify soft tissue among other tissues and at interfaces between two adjacent soft tissues in contact with blood or other physiological fluids. Therefore, radiopaque CAs, which are known as cold markers, are generally involved. To date, the sensitivity of X-ray scanners to traceable radiopaque probes remains slightly low. Typically, a difference of 50–100 HU leads to easy differentiation of

adjacent compartments and can be achieved by administration of a significant dose of a CA [20, 33, 34, 41–43].

### Radiopaque Contrast Agents for X-Ray Scanner Imaging

Typically, X-ray scanners find a key role in imaging various tissues by means of the administration of clinically approved (by the “Food and Drugs Administration” (FDA), an

**Fig. 4** Types of microscopic computed tomography with their typical in vivo scale at which investigation can be performed (reproduced with permission from [34]).



American organization in charge of public health protection) radiopaque substances, as reported in Table II.

To ensure good local contrast, radiopaque CAs, also known as radiographic CAs or roentgenographic agents, are utilized in X-ray imaging diagnostic procedures and accordingly are intended to accumulate and concentrate in a desired target. Radiopaque CAs have undergone significant evolution over the decades from the 1920s to 1970s. As briefly described in Table I, contrasting media for X-ray attenuation can be formulated with heavy elements capable of attenuating X-rays, such as the lanthanides cesium (Ce), gadolinium (Gd), terbium (Tb), dysprosium (Dy), ytterbium (Yb) and lutetium (Lu); the halogen iodine (I); the alkaline earth metal barium (Ba); the actinide thorium (Th); the post-transition metals lead (Pb) and bismuth (Bi); and the transition metals gold (Au), tungsten (W), tantalum (Ta) and rhenium (Re) [29, 33]. Many elements, such as thorium [45], a radioactive element, and formulations were tried before being withdrawn from in vivo radiography application or being replaced by safer compounds because of toxicity and immediate and delayed adverse side reaction concerns (such as skin rashes, nausea, headache, allergy, painful injection, thyroid dysfunction, nephropathy, renal toxicity, cardiovascular issue) due to their compositions and/or formulations with high osmolality and viscosity. It should be mentioned that as CAs are used in high doses, there are some patients for whom X-ray CT is contraindicated, for example, patients with renal failure, severe diabetes, and iodine sensitivity [46, 47]. Currently, oral barium sulfate suspension for GI investigation and injectable small water-soluble iodinated molecules for intravenous administration are mostly used. Increasingly, iodine has become an appealing element, even for GI visualization, because it avoids harmful in vivo effects and is inexpensive. Salts, such as sodium iodine or lithium iodine, were first tried as radiopaque tracers but turned out not to be convenient due to charge separation once exposed to in vivo fluids. Several attempts at formulations with iodine, ranging from ionic with high osmolality to nonionic with low osmolality, were also made. Ultimately, low-molecular-weight (< 2000 Da) and hydrosoluble iodinated molecules with triiodobenzene

group(s) have emerged as the best compromise between contrast enhancement and side effects [3, 20, 29, 31, 33, 42]. Typical iodinated molecules used as commercially available CAs are displayed in Fig. 5.

Aromatic molecules are more stable than aliphatic ones, and similar observations have been made with nonionic organic molecules. When ionic organic molecules were employed as contrast media, most molecules were positively charged to promote electrostatic interaction with in vivo entities (cells, proteins...), which are mostly negatively charged. Initially, this property seemed an asset to get closer to in vivo materials, but it turned out that those compounds had severe adverse effects on patient health, such as neurotoxicity and hemodynamic issues. As a result, focus shifted to injectable nonionic and aromatic iodinated molecules, and efforts were also made to improve biotolerance and toxicity [3, 20, 29, 31, 33, 42]. Nevertheless, these probes still exhibit some drawbacks directly correlated to their physicochemical properties. Blood-pool contrast media must be soluble in aqueous environments to be intravenously injected and distributed to tissues. Because of their hydrophilic characteristics, molecules suffer from fast renal excretion. Because of the poor sensitivity of X-ray scanners to detect probe signals, a high dose must be administered; however, high doses may cause acute renal toxicity. In addition to nephropathy and cardiovascular problems and allergic reactions because of iodine, this technique cannot be monitored, so MRI is performed as an alternative. The high osmolality and viscosity of some radiopaque CAs make this dosage form difficult to handle. A new class of lipid-based radiopaque active materials for in vivo targeting are replacing hydrophilic iodinated contrast agents. The formulations Lipiodol® [41] and Fenestra® [48], which are already on the market, have the same characteristics as those mentioned above. Nanotechnology-based CAs are also emerging on the market as a new type of CA [1, 3, 20, 30, 34, 42, 49, 50]. The emerging technologies using the CT modality are based on new applications, such as the assessment of rapid surgical margins in breast-conserving surgery [51, 52], noninvasive detection of coronary inflammation [53], parasite imaging [54], or determination of primary tumor dimensions in breast cancer specimens according to intraoperative micro-CT [55].

**Table II** Summary of Body Systems and Their Diagnostic Procedures by X-Ray Imaging with Contrast Enhancers [3, 20, 29, 44]

Body system	Organs or tissues (Procedure)
Vasculature	Vessels (angiography), arteries (arteriography), veins (venography), chambers of the heart (ventriculography)
Organs	Brain (brain CT), liver and spleen (abdominal CT), kidney (pyelography), gallbladder (cholecystography)
Spinal canal	Spine, lumbar, thoracic, cervical, total columnar (myelography), brain (cisternography)
Urinary track	Bladder (urethrography)
Gastrointestinal track (GI)	Upper GI including buccal cavity pharynx, esophagus, stomach, and duodenum and lower GI corresponding to small and large intestines
Joints	Joint (arthrography), disks (discography)
Uterine cavity	Uterus and fallopian tubes (hysterosalpingography)

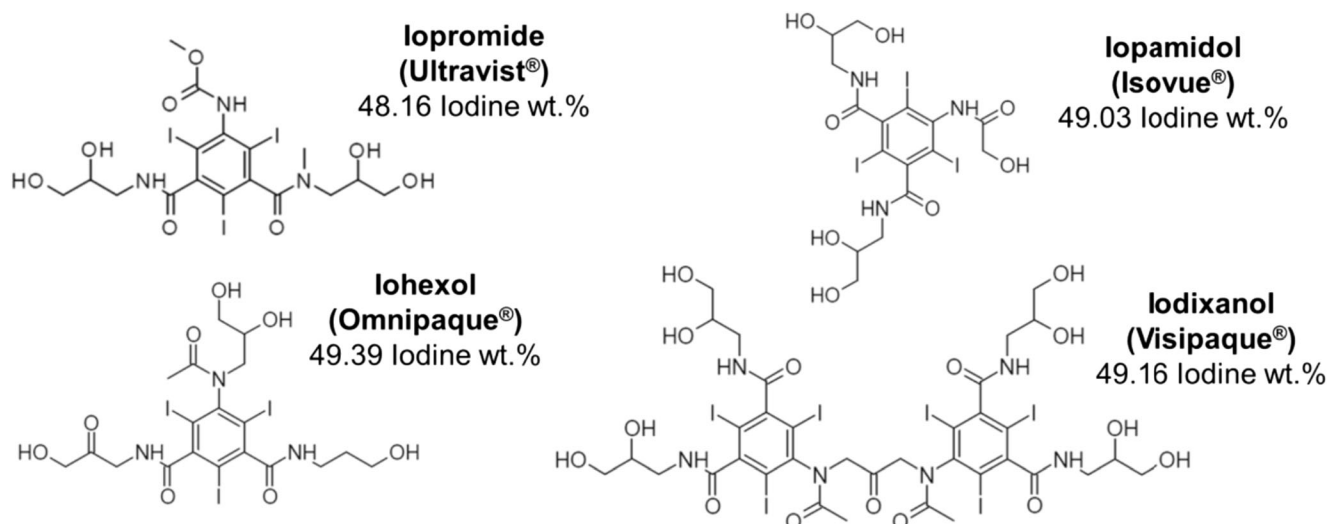


**Fig. 5** Chemical structure of representative commercial nonionic iodinated CAs with their commercial name and iodine content.

As we have well-developed scanners, the current emphasis is on improving the effectiveness of the CAs. Several requirements should be met to prepare an optimal iodine-based injectable preparation:

- The content of radiopaque elements, such as iodine, should be high to promote good X-ray attenuation (high iodine-to-particle or iodine-to-molecule weight ratio), and the material used should be biocompatible, inert with respect to tissues and chemically stable in physiological media;
- The formulation should be designed to prevent as many potential side effects as possible on patient health;
- The administration should be pain-free, and the viscosity, osmolality and pH should be compatible with intravenous injection, the blood-pool environment and in vivo fluids;
- The radiopaque substance should, once administered, have specific biodistribution to yield to local contrast enhancement within the zone of accumulation;
- The time of retention within the ROI should be long enough to avoid injection of a high dose, but the compound should be finally excreted after a significant amount of time without producing harmful metabolites.

The following section aims to introduce the second diagnostic tool, MRI. Similar to the X-ray scanner, the principles, main characteristics and CAs will be presented.

## MRI IMAGER

### History of MRI Scanner

For many decades, it has been well known that magnetic fields can cross human tissues without causing any harmful adverse effects on living organisms bearing no magnetizable materials

[56, 57]. Since then, the use of magnetic fields has been extended to biomedical applications such as those in the diagnostic and therapeutic domains (drug and gene delivery, hyperthermia cancer therapy, magnetic separation, etc.) [56–59]. Initially inspired by nuclear magnetic resonance, MRI is currently one of most well-developed magnetism-based techniques for human visualization. The MRI technique has improved rapidly and become one of the most famous tools for diagnosis [60]. First, MRI was known as nuclear magnetic resonance tomography. In 1971, R.V. Damadian opened a new route to improve cancer diagnosis using NMR technology [61]. On the basis of this new method, works by P.C. Lauterbur and P. Mansfield, who shared Nobel Prize in Physiology or Medicine in 2003 for their discoveries, and then A.N. Garraway's study led to the creation of 2D images by NMR in the 1970s [62, 63]. The first small laboratory animal was then imaged, and the first abdominal investigation of the human body [64] occurred quite soon after that. Later, the first clinical MRI was established in 1980 and produced its first images of the whole body in W.A. Edelstein's study [65, 66]. Real-time imaging techniques emerged finally by the end of the 1980s [67].

### Principle of MRI

MRI is actually a noninvasive and nonionizing imaging technique providing 3D images of deep and soft tissues with high resolution, and it is mostly used for the detection of tumors and their metastases, for observation of the brain and nervous system or for the evaluation of cardiovascular functions. MRI aims to provide images by evaluating the relaxation times (longitudinal T1 and transverse T2) of water molecules exposed to a magnetic field and radiofrequency pulse. Due to their location in different tissues, each compartment would have water molecules with their own relaxation speed [1, 56,



57, 60, 68]. Figure 6 collects general physical phenomena at the origin of the NMR signal from water molecules during an MRI procedure.

As illustrated in Fig. 6, MRI relies on the ability of protons from water in human body tissues to respond to a large magnetic field ( $B_0 > 2$  T) and a transverse radiofrequency pulsed sequence (5–100 MHz). Although the magnetic moment of water molecules is small, the large number of water molecules within biological media leads to a measurable effect due to the collection of all signals of hydrogen nuclei once exposed to  $B_0$ . Similar to the proton NMR principle, applying a magnetic field  $B_0$  causes magnetic moments or spins of hydrogen to align along the  $B_0$  axis (z-axis), which are not static but spin about  $B_0$  at the precession frequency (Larmor frequency  $\omega_0$ ). Then, radiofrequency pulses are introduced to proton nuclei, which absorb the energy and make the net magnetization ( $M_z$ ) of each spin switch from the z-axis to the xy-plane ( $M_{xy}$ ). When the transmission of the radiofrequency pulse ceases, the magnetic moments relax in a coherent response and process at the Larmor frequency to return to aligning along  $B_0$ . Thus, relaxation times are measured, then treated by Fourier transform and provide signals to build 3D images [56, 57, 59, 68].

### Origin of MRI Contrasts

Relaxation is actually based on two phenomena: i) longitudinal relaxation, commonly called T1 relaxation or T1-recovery

and “spin-lattice” relaxation due to the dissipation of the absorbed energy from radiofrequency pulses to the surrounding tissues, and ii) transversal relaxation, generally named T2 relaxation or T2-decay and “spin-spin” relaxation because of the loss of phase coherence by spin-spin interactions during spin precession. As implied, longitudinal and transverse relaxations are characterized by relaxation times, namely, T1 and T2, respectively [2, 56, 57, 59, 68]. Whereas T1 corresponds to the time to release 63% of longitudinal magnetization from spin to the surrounding media, generally as energy-like heat, T2 is the time that transverse magnetization needs to decrease by 37% [57]. Figure 7 shows an example of curves of  $M_z$  and  $M_{xy}$  net magnetizations as a function of time measurement, allowing us to estimate T1 and T2.

Furthermore, as mentioned above, longitudinal and transverse relaxations are two parallel magnetic phenomena that provide their own type of contrast: T1 recovery and T2 decay have brightening (positive contrast, hyperintense signal) and darkening (negative contrast, hypointense signal) effects, respectively [1]. Regardless of the differences in contrasting effects between T1 recovery and T2 decay, it must be noted that MRI contrast is related to the magnetic behavior of only one species, the protons. However, some variations in T1 and T2 within organs and the regions surrounding organs are noticeable, which means that protons do not act in the same fashion. Because of differences from one tissue to another, such as the composition and density, the spins will not relax at the same time since they will not be subjected to similar interactions

**Fig. 6** Schematic illustration of the MRI effect on the magnetic moment of hydrogen nuclei from water molecules contained in tissues to yield reconstructed images.

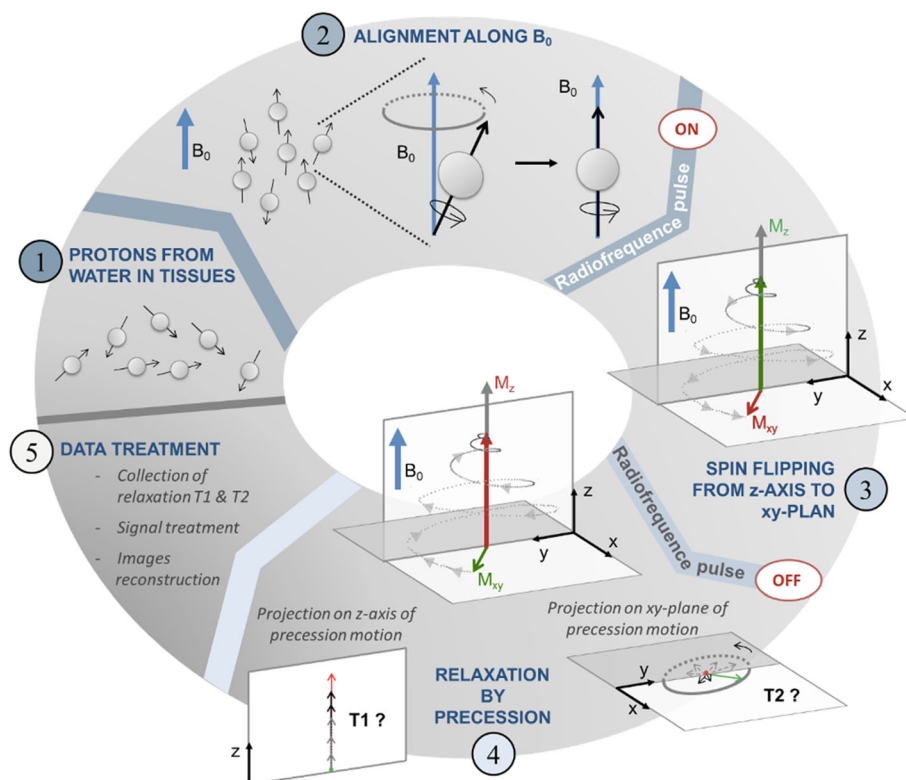
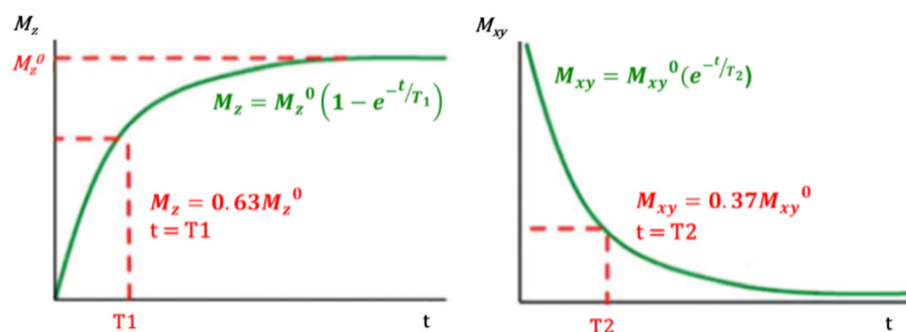


**Fig. 7** Curves of the relaxation process. Determination of (left) T1 longitudinal relaxation time and (right) T2 transverse relaxation time (reproduced with permission from [68]).



within their respective tissues [48, 60]. The last phenomenon to highlight with regard to the MRI relaxation process is the dephasing mechanism occurring during spin-spin relaxation because of magnetic field inhomogeneity within tissue, which is notably detected during T2-weighted MRI imaging of in vivo entities with a high payload of paramagnetic components. This new relaxation decay is described by the T2\* transverse relaxation time and provides subsequent information for functional MRI and perfusion imaging. Consequently, T2\* is even more sensitive to reveal macroscopic magnetization than T2 [69, 70].

However, like all imagers, contrast enhancement for MRI needs to be improved by means of introducing magnetic materials as CAs. Because the possibility of obtaining images with, on the one hand, brightening and, on the other hand, darkening depends on the measurement of T1 and T2, respectively, two families of MRI contrast media exist.

### Magnetic Probes for MRI Contrast Enhancement

Although MRI is an advanced technology and provides much more accurate images than other modalities, contrasting materials can be associated with improved contrast enhancement of some specific in vivo compartment by being near or within it. MRI relies on the magnetization of protons to provide signals that can be converted into accurate images of the inside of a living organism. Obviously, MRI CAs are magnetic compounds for both types of contrast, namely, for the so-called T1-weighted MRI and the T2- and T2\*-weighted MRI [71, 72]. Two categories of CAs are prevalent: gadolinium-based CAs for T1-weighted MRI and iron oxide-based CAs for T2 and T2\*-weighted MRI. Both kinds of MRI probes are nanoparticles (NPs), more precisely coated NPs, and therefore belong to the nanotechnology and nanomedicine fields. In fact, the use of nanoparticles as CAs for not only for MRI but also other imaging modalities derives from the fact that they present numerous advantages and high efficiency. The specific properties, strengths and limitations of NPs will be described in detail in section 5 and related to future trends in nanomedicines. In brief, the strong advantage of NPs lies in their ability to increase the circulation time in the

bloodstream, target specific sites, and encapsulate CAs and/or deliver active ingredients.

The first category is currently widely used in clinics. Many substances are already FDA approved, and some are described in Table III. There are two subcategories for gadolinium-based CAs: i) extracellular fluid agents for perfusion imaging (lymphatic system and vessels) and interstitial and intravascular space imaging and ii) blood-pool CAs, which are mostly for intravascular space and angiography investigations. Moreover, as shown in Table III, gadolinium-based CAs are intended mainly for fluid compartment and extracellular space imaging, whereas some more versatile CAs target specific tissues such as the liver, spleen, or lymph nodes, etc. With oral and gaseous CAs, the GI tract and lungs can also be visualized.

Gadolinium in its ionic form  $Gd^{3+}$  is included in CA formulations. As a free paramagnetic metal ion,  $Gd^{3+}$  has undesirable biodistribution and a relatively high toxicity (exchange with in vivo cations, dysfunction of enzymes and the reticulo-endothelial system (RES), deposition in tissues and bones). However, owing to its ability to reduce T1,  $Gd^{3+}$  has been complexed with various ligands to overcome its inherent and unfortunate issues for in vivo applications.  $Gd^{3+}$  chelates have high kinetic and thermodynamic stabilities and yields, enabling imaging of different interstitial spaces imaging upon administration as contrasting media for MRI depending on the nature of the ligands. Importantly,  $Gd^{3+}$  chelates are hydrophilic species that do not pass through the blood-brain barrier and are intended mostly to enhance the contrast of brain vessels and tumors. Their physicochemical properties allow them to be filtered by the kidney and to be consequently excreted by renal clearance before any potential gadolinium leakage. Elements other than lanthanides may also represent good candidates, for instance, transition metal elements ( $Mn^{2+}$ ,  $Fe^{3+}$ ,  $Cu^{2+}$ ...) or metal alloys due to the large number of unpaired electrons, providing paramagnetic ions suitable for T1-weighted MRI. Thus far, gadolinium-based compounds remain the most common CAs for positive contrast imaging. Nevertheless, their stability should be ensured to prevent  $Gd^{3+}$  leakage. Much attention has been devoted to ligand selection, for example, linear or macrocyclic and ionic or nonionic, and the  $Gd^{3+}$  core-to-ligand ratio to ensure

**Table III** Examples of Gd<sup>3+</sup> chelate T1-Weighted MRI CAs Commercially Available and Their In Vivo Target [42, 71–74]

Commercial Gadolinium-based CAs	Organs or tissues
Gadopentetate dimeglumine (Magnevist®) Gadoterate meglumine, (Dotarem®)	Central nervous system (CNS) (for blood-brain barrier, tumor, or spine imaging), whole body
Gadoteridol (ProHance®)	
Gadodiamide (Omniscan®)	CNS, abdominal cavities
Gadobutrol (Gadovist®)	CNS
Gadobenate dimeglumine (MultiHance®) Gadoversetamide (OptiMark®)	CNS and liver
Gadoxetic acid (Primovist® or Eovist®)	Liver
Gadofosveset (Vasovist®)	Abdominal cavities, limb vessels, vascularization

efficient Gd<sup>3+</sup> trapping. Patients suffering from kidney dysfunction or failure may not receive such probes. Special caution must be taken in this particular case to avoid nephrogenic systemic fibrosis, a chronic complication. Acute side effects may happen soon after administration, but they are not severe and are manageable (nausea, dizziness, itching from intravenous injection, chills, headache) [57, 68, 71, 73–75].

The second class, the T2- and T2\*-weighted CAs, is also present on the market but is not as commonly available as T1-weighted CAs. Iron oxides are generally magnetite and/or maghemite phase, Fe<sub>3</sub>O<sub>4</sub> and γ-Fe<sub>2</sub>O<sub>3</sub>, respectively. In fact, iron oxide NPs (IONPs) have been studied and developed as MRI tracers for 30 years, whereas gadolinium has been introduced only recently [68]. Indeed, some concerns are still mentioned in the literature about IONPs due to the lack of knowledge on their in vivo fate [76]. Similar to T1-weighted CAs, all T2 and T2\*-weighted MRI CAs approved by FDA are coated IONPs, as shown in Table IV. Depending on the physicochemical properties of the coating, also called the outer shell, the biodistribution of the introduced IONP-based CAs is different. In addition, the overall size is also a key parameter that can promote accumulation within a desired or at least local ROI.

To clarify, IONP is a general term to refer to families of IONPs in different size ranges: microsized paramagnetic IONPs (few micrometers), superparamagnetic IONPs (SPIONs) (~100 nm), ultrasmall IONPs (USPIOs) (<50 nm) and monocrystalline IONPs (10–30 nm) [57, 72, 75, 81]. As indicated by the CA descriptions in Table IV, the smaller the IONPs are, the higher their specific surface, and thus, the better

their interactions with the surrounding bulk phase. Indeed, depending on their size, these nanoprobe are basically used to provide negative contrast for the liver and spleen (50–100 nm SPIONs) or for lymph nodes and bone marrow (<50 nm USPIOs). The smallest IONPs are capable of extravasation through the capillary system and are not subject to opsonization. Consequently, the in vivo biodistribution and bioaccumulation of decorated IONPs are not only based on surface chemistry but also dependent on size [1, 56, 57, 59, 68, 75, 81].

Consequently, compared to T1-weighted CAs, IONP CAs are more suitable for perfusion imaging because of their very small dimensions and for soft tissue imaging [1, 59, 68, 77, 79]. For instance, owing to their ability to be opsonized by RES cells such as Kupffer cells located in the liver parenchyma, pathological tissue in the hepatic area is easily diagnosed. Although the consequence of phagocytosis is excretion upon metabolization (opsonization mechanism) of the contrasting materials, such sequestration of IONPs allows efficient liver mapping to detect unhealthy cells and a lack of RES cells among healthy cells [1, 59, 68, 77, 79]. As a result, IONP CAs are eliminated by the hepatic route but also through the splenic route, in contrast to gadolinium compounds, which are removed from the body by the urinary pathway. Although the clearance mechanism of IONPs is still debated, metabolization of iron oxide may promote the formation of a non-superparamagnetic ion form, which may then become part of the normal iron pool and be incorporated into red cells or involved in other in vivo processes and entities (hemoglobin, ferritin). Few side effects of CAs on the market are also mentioned in the literature, such as hypotension,

**Table IV** Examples of Commercially Available IONP-Based T2-Weighted MRI CAs, Their In Vivo Target and the Size of the IONPs Included Within each CA FORMULATION [57, 59, 77–80]

Commercial iron-oxide-based CAs	Target	IONPs size (∅)
Ferumoxsil (Lumirem® or GastroMark®) - Silicon coating Ferristene (Abdoscan®) - Sulfonated styrene-divinylbenzene copolymer citrate coating	Bowel, lumen organs	300 nm > ∅ > 3.5 μm
Ferumoxide (Endorem®) - Dextran coated-Fe <sub>3</sub> O <sub>4</sub> Ferucarbotran (Resovist®) - Carboxydextran coating	Liver, spleen	80 nm < ∅ < 180 nm ∅ = 60 nm
Ferumoxtran-10 (Sinerem® or Combinex®) - Dextran coating	Lymph node	20 nm < ∅ < 40 nm
Feruglose (Clariscan®) - PEG starch coating	Bone marrow, perfusion, vessel	∅ = 20 nm

lumbar pain, leg pain, vasodilatation and, in very rare cases, paresthesia. Toxicity issues, usually based on potential interactions with nanoscale in vivo entities and IONPs, are also still debated [1, 77, 79, 80].

The contrast and efficiency of paramagnetic and superparamagnetic CAs in surrounding tissues is related to their impact on relaxation times. For this purpose, the contrast-enhancing efficiency of an MRI CA is expressed through longitudinal and transversal relaxation  $r_1$  and  $r_2$ , respectively (expressed in  $\text{mM}^{-1}\cdot\text{s}^{-1}$ ). Such parameters are defined as the increase in relaxation rate ( $1/T_1$  or  $1/T_2$ ) of water protons induced by 1 mmol/L active iron. To determine if a CA is more suitable for T1- or T2-weighted imaging (and thus for T2\*-weighted MRI), the  $r_2/r_1$  ratio has to be evaluated: the higher the  $r_2/r_1$  ratio is, the greater the product contrast for T2-weighted imaging ( $>10$ ). Experimentally,  $r_2$  and  $r_1$  are obtained from plots of  $1/T_1$  and  $1/T_2$  versus the iron concentration, and the following equation correlates the relaxation rate and concentration and provides  $r_1$  and  $r_2$  as the slope:

$$\frac{1}{T_i} = \frac{1}{T_i^0} + r_i C \quad i = 1, 2 \quad (2)$$

where  $T_1$  and  $T_2$  are the longitudinal and transverse relaxation times, respectively;  $T_1^0$ ,  $T_2^0$  are the relaxations in pure water;  $r_1$  and  $r_2$  are the relaxivities; and  $C$  is the concentration of the active element within the CA formulation [58, 68, 75]. An example of such a plot is depicted in Fig. 8.

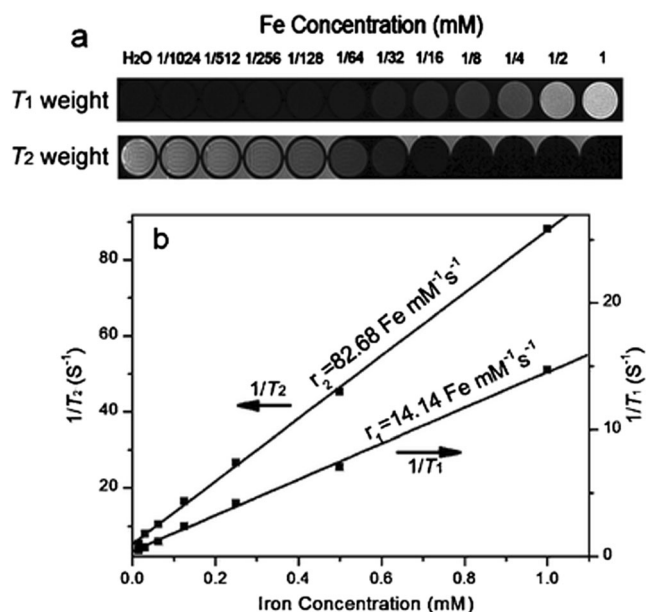


**Fig. 8** Example of  $r_1$  and  $r_2$  measurements. (a) T1-weighted and T2-weight in vitro MRI images of aqueous solutions at different Fe concentrations and (b)  $1/T_1$  and  $1/T_2$  plotted against Fe concentration (reproduced with permission from [82]).

To further improve the current paramagnetic and superparamagnetic contrast formulations and prepare the optimum injectable preparation, a few requirements should be met:

- The content of paramagnetic and superparamagnetic elements, such as  $\text{Gd}^{3+}$  and IONPs, should be high enough to promote good contrast enhancement, and the material used to coat or chelate the active element should be biocompatible, should be inert with respect to tissues and should confer stability to complexes and NPs in physiological media;
- Formulations should have limited adverse effects on patient health;
- The formulation should be well designed to prevent  $\text{Gd}^{3+}$  leakage by trapping with suitable ligands or large IONP use to avoid embolism of small vessels;
- The administration should be pain-free, and the viscosity, osmolality and pH should be compatible with intravenous injection or oral administration, the blood-pool environment and in vivo fluids;
- The radiopaque substance should, once administered, have specific biodistribution to yield to local contrast enhancement within the ROI;
- The retention time within the ROI should be long enough to administer a tolerable dose, but the compound should be ultimately excreted after a significant amount of time without producing harmful metabolites;
- Special care should be taken concerning the ROI (fluids space, organs, and lesions) to determine which image weighting is more suitable, and then an appropriate CA compatible with the patient's health condition should be found.

To conclude on MRI, X-ray scanners and their corresponding probes, it must be noted that both modalities remain important and efficient tools for noninvasive and early-stage diagnostic practice. On the one hand, the main modality used, the X-ray scanner, has some inherent drawbacks, such as radiation exposure and iodine allergy, prohibiting some patients from being subjected to X-ray scanning with contrast enhancer administration. On the other hand, MRI may constitute a more expensive and more accurate alternative for such patients. However, it should be considered that this modality is not indicated for all patients (e.g., for those bearing implanted magnetizable devices). The types of CAs are based on NPs or complexes for which stability and in vivo fate should be comprehensively studied. As a result, both techniques are required and may be used in combination to obtain complete and unambiguous diagnoses. Their limitations thus need to be overcome, and the development of new unimodal and bimodal CAs would be a very interesting first step to render diagnostic procedures by imaging easier for patients.

The next section will focus on present-day needs for clinical imaging and the CAs associated with MRI and X-ray scanners. The following part aims to highlight the importance of moving forward in research in the noninvasive diagnostic field and how it can be carried out by pursuing advances at the preclinical stage. Promising and emerging preclinical probes based on nanoparticulate systems will be introduced for both modalities.

## CURRENT LIMITATIONS AND CHALLENGES: AN INCREASING NEED FOR A NEW GENERATION OF CONTRAST AGENT FOR PRECLINICAL AND CLINICAL IMAGING

### Multimodal Imaging: Combination of Independent Imaging Results

As noted in the last section, one modality can be replaced by another in cases of incompatibility with patients' health. Other circumstances may lead to switching from technique to another: the most common reason is the need for complementary information. Increasingly, the literature shows studies on applications of one, two or three imaging instruments to combine their independent data at their own scale, as shown in Fig. 9.

Much more details about disease, treatment efficacy and biochemical processes can be obtained by involving several imaging strategies for the exploration of the ROI. This aim will improve the diagnosis process; to this end, findings from each imaging modality will be validated, interlaced and correlated. In addition, this multimodal approach is based on exploiting strengths and compensating weaknesses of current imaging techniques [5, 6, 50, 84]. For instance, near-infrared fluorescence and MRI were combined for breast cancer detection using multivalent traceable probes. The high probe sensitivity of optical imaging allowed a quick overview of probe accumulation within the tumor to be obtained, and T2-weighted MRI provided excellent delineation of the tumor structure, including the margin and necrotic zones [85]. The same combination of optical imaging along with MRI was chosen to detect epithelial cancer cells [86]. Other studies also used a bimodal imaging approach with MRI/X-ray scanners to image the complete tumor vasculature [83], as illustrated in Fig. 9 (left), or for embolization follow-up [87]. Trimodal imaging is also increasingly common; for example, optical/MRI/X-ray scanners were used for *in vivo* liver imaging and detection of probe internalization by liver cells (Fig. 9 (Right)) [88].

### Towards Novel Preclinical Probes with Additional Features and Tunable Design

All these promising combinations of modalities might become potential breakthroughs for the preclinical diagnostic field

and, later on, for clinical translation. Indeed, not only would diagnostic processes be even more efficient and accurate, but novel treatment strategies could also be imagined. Improving the retention time and accumulation of probes, which remains one major limitation of iodinated CAs on the market, might enable visualization of the ROI over a longer period. Consequently, tissues and lesions could be monitored as long as the CA remains accumulated. In the case of treatment response monitoring and extended retention within the investigated ROI, avoiding repeated administration of CAs is an important quality. Therefore, novel fields such as the theranostic field, which is based on drug release, treatment efficacy follow-up and imaging, are now increasingly developed and are currently well documented in the literature [89–91]. The so-called theranostic platform aims to design delivery systems that carry therapeutics and imaging compounds. It involves a system with an architecture allowing that system to carry pharmaceuticals or active pharmaceutical ingredients (APIs), such as CA(s) and drug(s), that is, a system with a multifunctional payload that can be transported within the blood pool, distributed to the ROI and then accumulated and/or released within the surrounding tissue [89]. Twinning CAs with therapeutics or treatment strategies has been adapted by many authors to apply different treatment strategies for specific diseases along with suitable imaging tools. For example, Barsanti *et al.* [92] explained how promising it could be to combine imaging CAs, mostly MRI probes and PET/SPECT radionuclides, with an API for diabetes management to observe pancreas, pancreatic cell or  $\beta$ -cell function and respond to antidiabetes treatment. A study on the detection of atherosclerotic ruptured plaque and antiangiogenic plaque therapy was also carried out, and a drug release study with an MRI follow-up was performed by encapsulating SPIONs within phospholipid cross-linked shells with controlled dissolution properties [93]. Other cases in the literature also report a theranostic strategy except without incorporating an API other than a CA. Recently, an overview described the advantages of dye-conjugated polymers for theranostic applications. These near-infrared-absorbing conjugated polymers were used to perform local photothermal cancer treatment. They were also identified as interesting nanoconstructs for doxorubicin drug release with a synergistic effect along with the photothermal treatment on tumors [94]. Another group used manganese ferrite NPs with a dye-doped silica coating as an MRI CA to locate the ROI, to visualize its anatomy and to apply hyperthermia treatment; a fluorescent dye was also implied to evaluate the treatment efficacy on cells [95]. Therefore, all multivalent probes mentioned directly above and dedicated to both imaging and therapy were actually designed into nanoparticulate systems, as illustrated in Fig. 10, as nanoassemblies for coencapsulating APIs and transporting them to a local ROI. Nanocarriers (NCs) and NPs offer efficient designs to overcome common

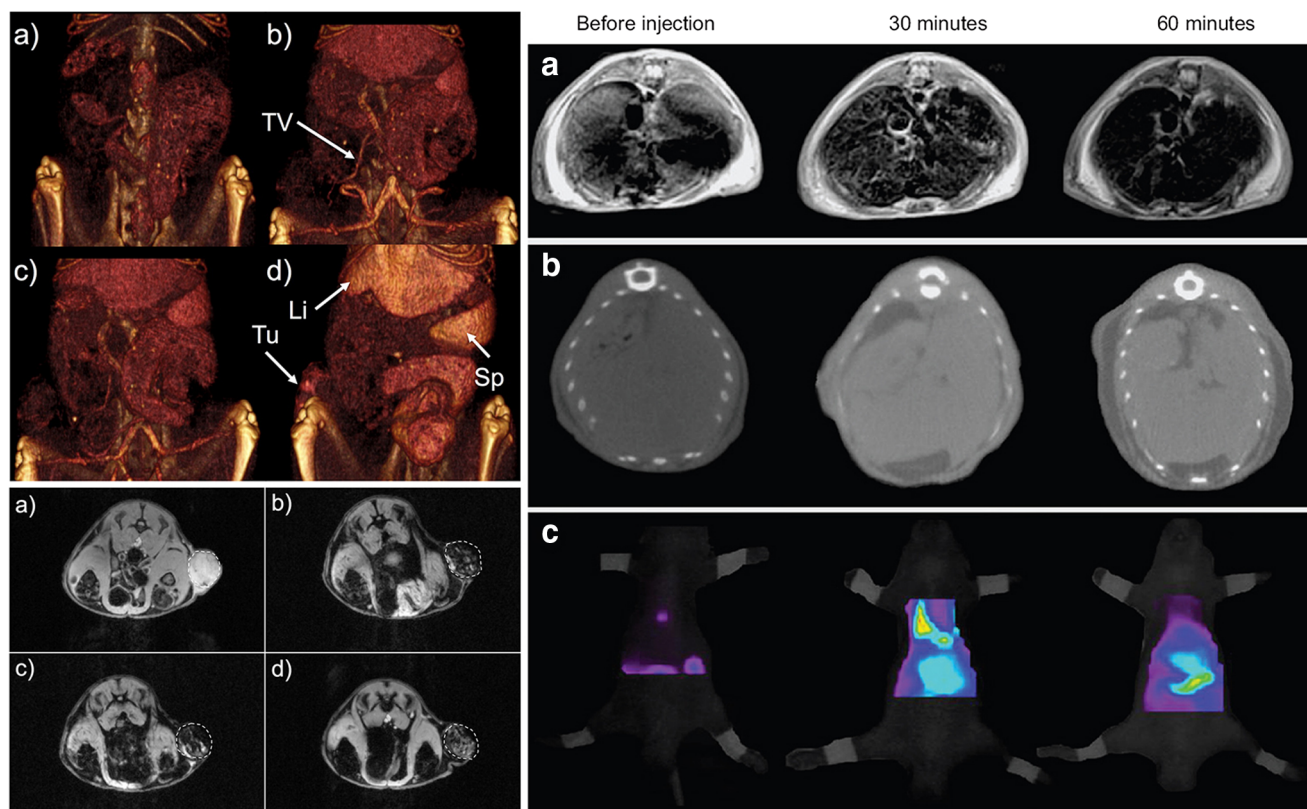


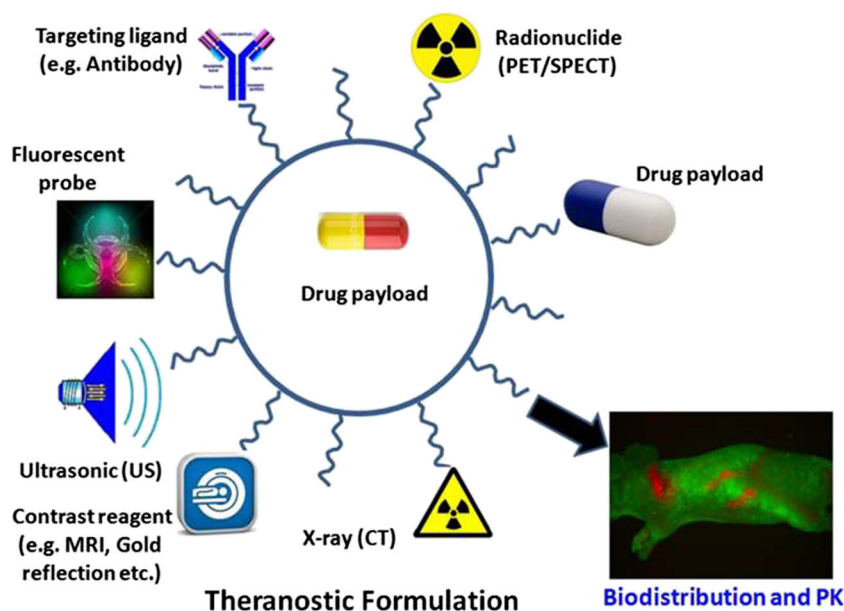
**Fig. 9** (Left) In vivo images of a rat bearing tumors by (top) X-ray micro-CT and (bottom) T2-weighted MRI a) before injection and (b) 1 h, (c) 2 h and (d) 24 h postinjection of a bimodal CA based on a SPION core coated with a tantalum oxide shell (TV, Li, Tu, and Sp indicate respectively the tumor vessel, liver, tumor and spleen). (Right) In vivo imaging by (a) T2-weighted MRI, (b) X-ray micro-CT and (c) fluorescence of trimodal probe biodistribution in the liver before and 30 min and 60 min postinjection (reproduced with permission from [83]).

disadvantages of APIs, such as low bioavailability (poor cell penetration, interaction with the ROI, selectivity for the ROI), poor solubility in the blood pool and lack of chemical stability once exposed to biosystems, by trapping them within their core. Importantly, the term multifunctionality covers a wide

range of functions (imaging, therapy, targeting, penetration within biological entities, stealth property and others), which can all be displayed in one versatile NC [96].

Although they are promising, all the abovementioned multifunctional probes were also designed as NPs because of their

**Fig. 10** Range of possibilities of preclinical multifunctional NPs as delivery systems dedicated to theranostic purposes. Targeting moieties might be incorporated on the NP surface for vectorization to promote specific biodistribution of NPs and interaction with selected ROIs. Imaging moieties aim to monitor NP accumulation at the targeted ROI and provide information about the pharmacokinetics (PK) and clearance mechanism (reproduced with permission from [89]).



applications for preclinical trials on small laboratory animals, which actually bring about difficulties for researchers owing to the animal model scale.

### Issue Regarding Scaling-up Nanoparticulate System-Based Contrast Agents from Preclinical to Clinical Applications

All multifunctional structures presented in previous examples were established with nanoparticulate designs. However, it must be highlighted that preclinical studies are mostly performed on small laboratory animals to ensure the safety of innovative pharmaceuticals such as CAs and to extend the use of current imaging modalities to more efficient diagnostic strategies for further human applications [35]. There are considerations regarding the welfare of animals (duration of anesthesia, temperature control, breath and heart monitoring, side effects, symptoms of pain or intolerance), but there are also technical hurdles to overcome, such as difficult vascular access and the small blood-pool volume [7, 38]. Because of the animal model scale, substances under preclinical study must consequently be administered in only limited volumes, be capable of avoiding or at least postponing the clearance mechanism (faster for animals than humans) and have a high loading of CAs and potential additional APIs to offer good contrast enhancement property once exposed to the *in vivo* environment [30, 49]. To fulfill these needs, NPs are perfectly adequate for such animal models and seem promising for scale-up due to their versatility as multifunctional probes. The optimum end of preclinical studies should be translation to clinical trials if they meet current needs and requirements (Fig. 11). However, even though NPs currently appear as a future generation of versatile probes for clinical use, translating such nanodevices to humans requires consideration of their behavior and *in vivo* fate once introduced into the human body. Clinical scale-up and translation to humans are indeed performed only once the CA or theranostic probe has received FDA approval after being tested during clinical trials [97, 98].

Consequently, NPs can be identified as the next generation of CAs and have some additional features to yield supplementary functions, such as for theranostic applications, to overcome the limitations of probes currently applied in the clinic. Despite concerns about the *in vivo* fate of NPs once administered into the human body, some NP-based CAs have nevertheless already been introduced into humans, such as MRI with SPIONs as contrast enhancers. As a result, NPs not only were found to be suitable for studies on animals but also are currently increasingly demanded for human model applications due to their huge potential as ideal probes because of their versatility.

To pursue this new trend, the following section will introduce NPs in depth, especially those dedicated to imaging via X-ray scanners and MRI.

## NANOPARTICLES AND NANOCARRIERS AS FUTURE MULTIFUNCTIONAL TRACEABLE PROBE PLATFORMS FOR IMAGING

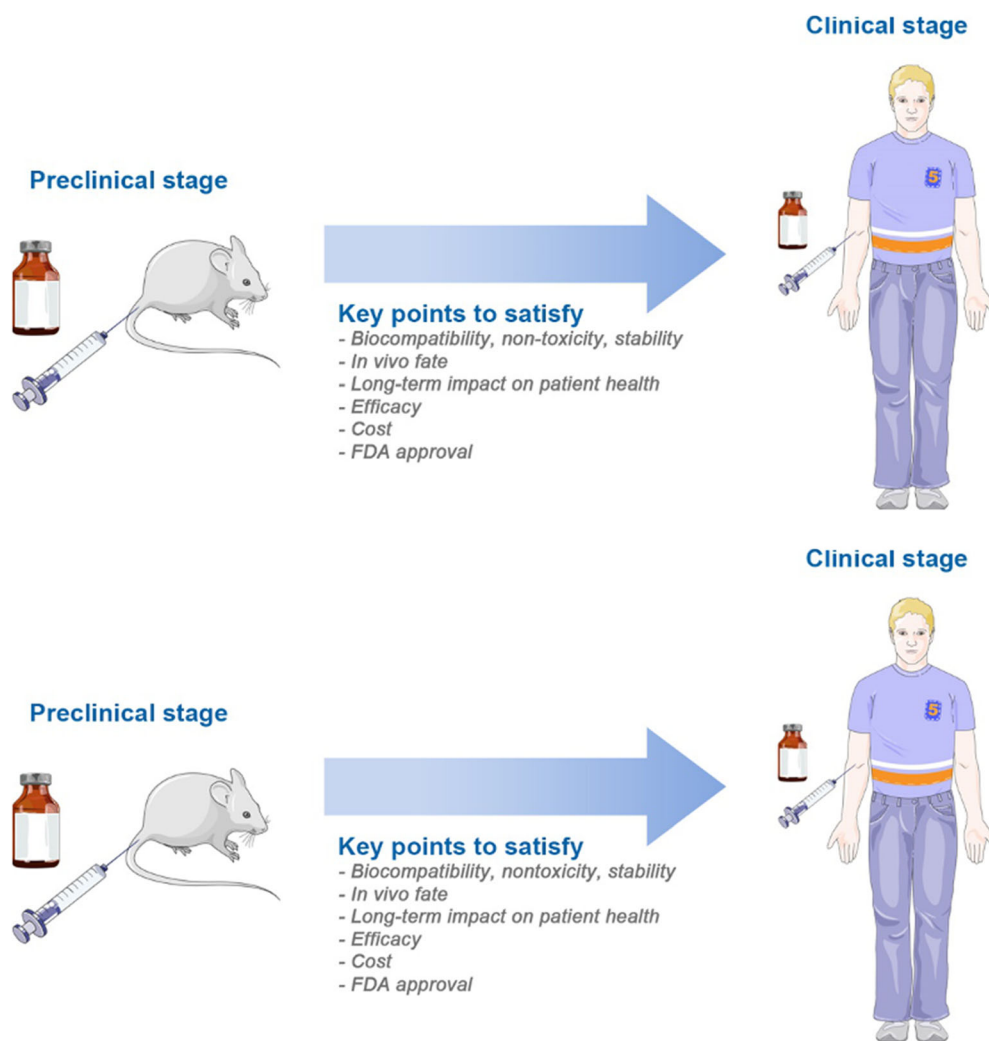
### Introduction to Nanoparticles

“Nano” derives from Greek and refers to tiny dimensions beyond the limit of visibility for the naked eye. Therefore, all objects described as “nano” are nanometric-sized entities. The term NP was used for the first time during the 1980s; before then, it was mentioned as a “small particle” [99, 100]. “Small particles” had been under investigation for more than a century at that time because their numerous size-dependent physical and chemical properties were appealing to researchers (including M. Faraday, who contributed work that explained the size and color of gold NPs [101]). After the 1980s, great interest arose from the scientific community, and thus, the development of nanotechnology has been devoted to nanoscience and nanomedicine applications [102].

The term NP includes all kinds of materials, such as organic, inorganic, hybrid, alloy, and composite. Furthermore, although they are usually produced with a spherical shape, NPs with other morphologies can be found, such as rods, cylinders, stars, cages and other geometries that are more or less complex (inhomogeneous NPs). The general definition of NP is a tiny particle with one of its dimensions between 1 nm and 100 nm [102]. As shown in Fig. 12, the nanoscale of NPs render them comparable to several biological entities, such as cells (10–100  $\mu\text{m}$ ), viruses (20–450 nm), genes (2 nm wide and 10–100 nm length) or proteins (5–50 nm), and allows them to get close to these entities (depending on features exhibited on their surface to promote specific interactions) [59, 102–105].

NPs are also referred in the literature as colloids when they are in dispersion or in suspension. Depending on the size of the NPs, a colloidal suspension allows light scattering to be observed. For light scattering to be observed, a few conditions must be met: i) colloidal matter with a radius in the range of the wavelength of light ( $\lambda$ ), that is, at the nanometer scale, and ii) good dispersion within the medium of dispersion, which must be iii) a light-transmitting medium (liquid, gas). Light scattering by NPs was also studied many years ago. It began during the nineteenth century with J. Tyndall, who was the first to become interested in turbidity, the so-called “Tyndall effect”, an optical phenomenon visible when large particles scatter sunlight [106]. Then, in 1908, G. Mie and L. Lorentz devised the Lorentz-Mie theory to describe light scattering by a nanosphere (radius ranging  $\lambda$ ) [107]. Finally, the last important law was from J.W. Strutt, 3rd Baron Rayleigh; Rayleigh scattering is actually a particular case of Lorentz-Mie theory applicable for NPs with a radius smaller than the wavelength of light ( $\lambda / 10$ ) [102, 108]. An example of light scattering by NPs is depicted in Fig. 13. Notably, this bluish

**Fig. 11** Translation of an NP-based CA from the preclinical to the clinical stage



aspect is a common qualitative characteristic that allows nanoscientists to quickly detect the presence of nanoscale particles in dispersion.

Another interesting fact about NPs is the high surface-to-volume ratio that confers a large surface available for anchoring or electrostatic attachment of ligands or specific moieties. The surface and size of NPs offer many opportunities to tune their chemical, physical and optical properties and, consequently, to design NPs with specific features for a desired application [34, 109, 110]. Figure 14 supports how the surface area increases with decreasing size. It also depicts that the number of atoms at the NP surface follows the same trend, providing a large number of atoms for potential chemical reactions and physical adsorption for surface tailoring purposes.

To keep establishing how the size of NPs is meaningful for NPs, it has to be mentioned that several properties are dictated by such parameters. For instance, colloidal stability requires Brownian NPs with efficient surface properties to achieve good dispersion. The surface of NPs is also size-

dependent because the smaller NPs are, the higher the surface area, and the more ligands that can be attached. In addition, colloidal stability is also related to surface charge and is a well-documented topic due to the old theory from B. Derjaguin, L. Landau, E. Verwey and T. Overbeek, known as DLVO theory [111, 112]. Although all information collected here was for both organic and inorganic NPs, it must be specified that in the case of inorganic NPs, many properties, such as magnetism as well as fluorescence in the case of quantum dots, are drastically impacted due to the quantum effect and surface area changes from bulk material to the NP scale. The case of magnetism is particularly interesting since it addresses inherent properties that are related to MRI and CAs [102, 103, 105, 113]. Finally, it is important to note that nanoparticles face a current reluctance regarding the “nanoscale” of these carriers, and the few solutions on the market are based on biocompatible materials, namely, lipids, for which all the degradation and metabolism processes have been extensively studied and the benefit-to-risk ratio has been considered acceptable. However, in view of the constant number of new



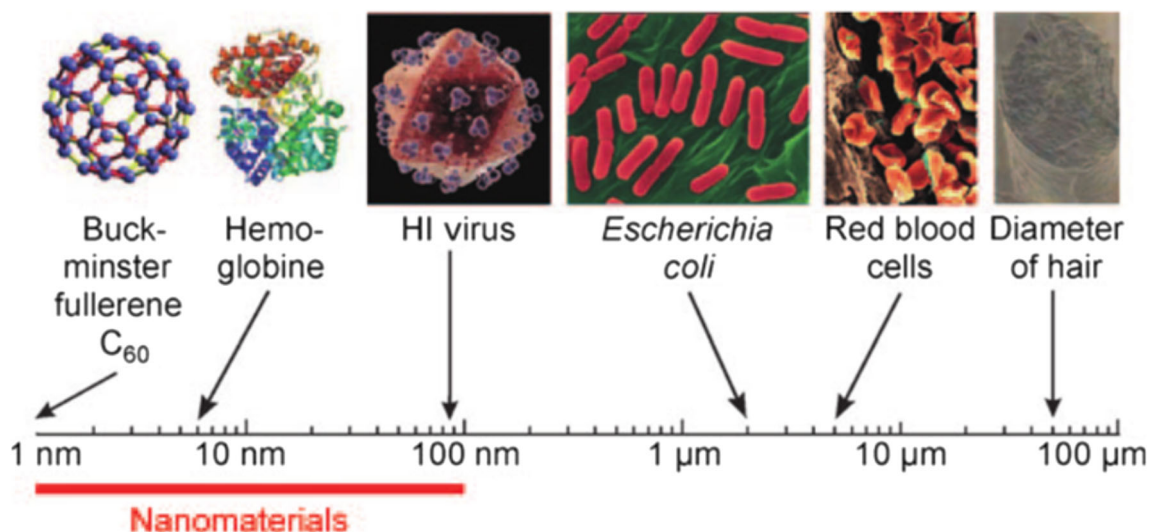


**Fig. 12** Length scale to compare NP dimensions to the size of biological materials (reproduced with permission from [102]).

nanoparticulate systems, new developments—discussed herein as well—of sophisticated solutions, NCs and potentially nanotheranostics still have important potential for imaging applications and targeted drug delivery. Even if some of the targeted NCs are eliminated by the liver or spleen in the case of efficient EPR or active accumulation at the target site, the local concentration may be sufficient enough to achieve the desired—therapeutics or imaging—objective, thereby bypassing (or decreasing) side effects because the total dosage is globally lowered.

The next section will outline NPs prepared for in vivo uses, especially for the field of diagnosis by imaging. Requirements and specifications related to biomedical concerns will be detailed to determine the characteristics of ideal nanoprobes.

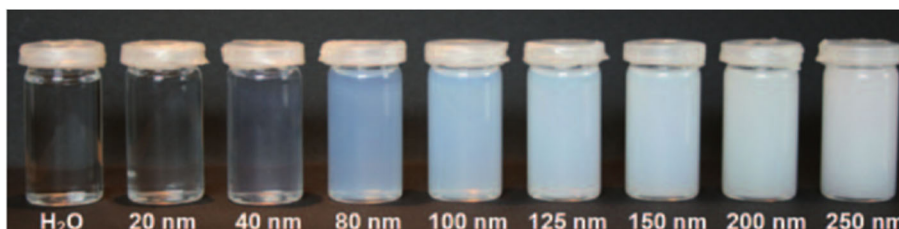
### Nanoparticles Dedicated to Biomedical Imaging: Requirements and In Vivo Concerns

NPs feature the ability, as introduced before, to form a drug delivery system (DDS) of an API due to their controllable and tunable design. They can indeed be easily adjusted to fit with the in vivo environment and contribute to advancing the nanomedicine field, including imaging and therapy strategies. NPs not only offer controlled release of API(s) but also provide confirmation of the site-specific delivery of the substance(s) by

incorporation of an imaging agent. In fact, NPs involved in biomedical applications are generally a double structure construct including a core and a shell and are also known as NCs. Therefore, NPs can be loaded with API(s) onto or into their core-shell assembly via encapsulation, surface attachment or entrapment. To carry their payload, which can be therapeutics, imaging agents or both, to a selected target, tailored NPs and/or NCs must bypass several biological barriers.

The human body has a very effective defense system to remove and protect itself against foreign xenobiotics. The immune system is one obstacle for NPs; indeed, upon administration, NPs encounter changes in pH, osmolality and ionic force that can alter NP constructs (agglomeration, physical degradation, modification of their properties). Their introduction into the bloodstream may also induce a negative host response, imparting potential premature clearance by opsonization or renal filtration from the organism. The in vivo fate of NPs once exposed to biological media is dictated by physicochemical properties. The typical biodistribution a few minutes after NP blood clearance is 90% in the liver, 2% in the spleen and 8% in the bone marrow, but the values remain highly dependent on NP characteristics. Likewise, biodistribution and pharmacokinetics can *ipso facto* be predicted by adjusting the design (size, shape, surface, targeting, composition) [50, 57, 114–117].

**Fig. 13** Light scattering optical phenomenon occurring in SiO<sub>2</sub> NP suspensions with various size distributions (reproduced with permission from [102]).



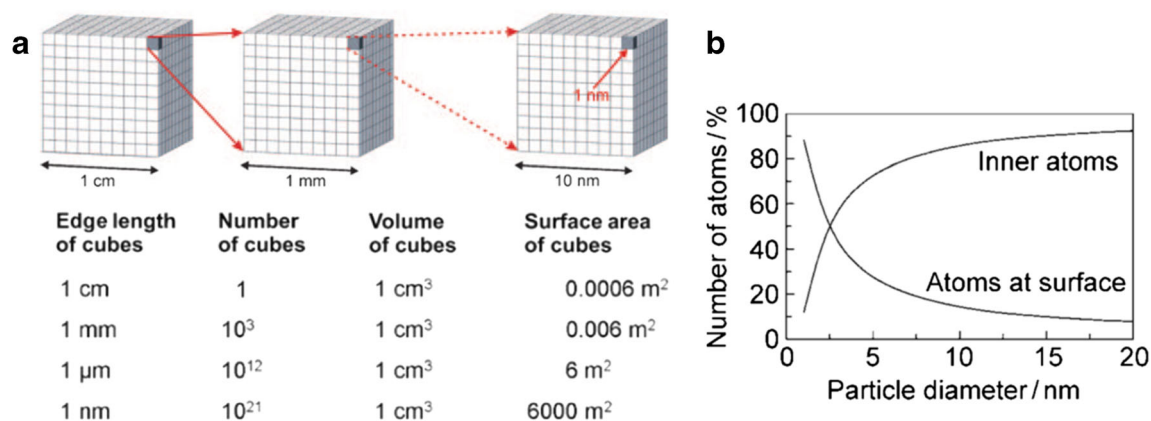


**Fig. 14** (a) Variation in the surface-to-volume ratio and (b) repartition of atoms vs the NP size (reproduced with permission from [102]).

## Size

The mean diameter of NPs is a key parameter governing the NP concentration in the blood pool and affecting the clearance process and biodistribution (extravasation through the tumor vascular system, permeability out of regular vasculature). Small NPs may be able to penetrate physiological barriers due their similar dimensions, gain access to many areas and avoid embolism outcomes. Typical NPs administered are smaller than 200 nm, whereas the smallest capillary pore diameter is approximately 2.3 μm. Using NPs for imaging has been attempted not only for preclinical testing on animal models but also for overcoming the fast elimination of hydrophilic iodinated CAs. Size is effectively the most impacting parameter to regulate NP-based CA elimination and accumulation. Basically, the largest particles (150–300 nm) will mostly be excreted by hepatic and splenic routes once an opsonization mechanism occurs. The optimization process is conducted by the RES or mononuclear phagocyte system (MPS), indicating plasma protein (opsonin) absorption as a biochemical signal of foreign entity intrusion. Sequestration and excretion of NPs are then carried out by phagocytic cells located in RES organs, such as Kupffer cells in the liver and macrophages in the spleen. To postpone MPS uptake and the subsequent clearance process, NPs must have high curvature, which means a very small hydrodynamic diameter. Nevertheless, NPs smaller than 20 nm will be subjected to renal clearance, whereas medium NPs (50–150 nm) will generally accumulate in bone marrow, heart, kidney and stomach [90, 114, 116–119].

## Surface Chemistry

Another prerequisite for long circulation times in the bloodstream and RES bypass is related to the NP surface properties. Surface decoration relies on surface charge, hydrophilic or hydrophobic properties, and conjugation of passive targeting ligands or active targeting moieties.

The simplest design of NPs is based on stealth and neutral NPs. Stealth properties imply the use of biocompatible and water-soluble polymers as flexible hairy shells, such as poly(ethylene glycol) (PEG). Both PEGylated amphiphilic macromolecules and dextran were used on SPIONs and USPIOs; excellent stabilization against opsonin absorption and low cytotoxicity compared to that of bare NPs were observed [120, 121]. Polyesters are also widely used, especially lactide and glycoside polymers and copolymers such as poly(lactic acid) (PLA), poly(lactic-co-glycolic acid) (PLGA), and poly( $\epsilon$ -caprolactone) (PCL), for DDSs because of their biocompatibility, low degradation rate and controlled drug release ability [122, 123]. Some other polymers are already on the market and used as coatings for long-term retention, such as poloxamer (Pluronic®), a triblock polymer (poly(propylene oxide) (PO) flanked with two hydrophilic PEG chains) and poloxamine (Tetronic®), a tetrafunctional block copolymer of PO and PEG [124, 125].

Many modified polymers have been applied, particularly for liposome NCs for passive targeting. It should be mentioned that liposome NCs were one the first PEGylated NC types marketed during the mid-1990s, when passive tumor-targeting DDSs of doxorubicin known as Doxil® or Caelyx® emerged. All these polymers act as hindrance shields, attracting water molecules as a cloud and thus fooling the immune system. Such a “chameleon effect” avoids premature opsonization and provides steric stabilization, preventing NPs from aggregating. Most often, a PEGylated shell is used to prolong the circulation time of NPs and reduce their cytotoxicity. Compared to passive targeting, the case of active targeting, detailed in the following section, is much more developed and involves a wide range of ligands (aptamers, peptides, vitamins, antibodies, small molecules). Changing the surface charge and hydrophilic properties may lead to a nonspecific interaction with biological entities, which are generally negatively charged. Positively charged NPs will have random binding with nontargeted cells, and hydrophobic NPs will encounter

aggregation issues in physiological media and will be cleared by the RES. It appears that optimum surface decoration would be neutral and hydrophilic [90, 96, 110, 114, 116–119, 126–129].

Figure 15 summarizes how surface properties and size ranges affect the biodistribution of NPs. Clearly, these two parameters are connected and must be well-controlled to guarantee NP accumulation in the ROI and evasion of *in vivo* obstacles.

### Shape

The effect of NP shape has not yet been well documented: a few studies have proved that NP biodistribution, *in vivo* interaction and toxicity were shape-dependent [130, 131]. However, a limited number of comparative studies are available to discuss the impact of nanorods, nanospheres, nanocubes, nanotubes, etc., on the pharmacokinetics of NPs. Hypothetically, the flexibility and hardness of the nanoconstruct might influence filtration and, consequently, the clearance mechanism [90, 114].

### Targeting

Vectorization of NPs is particularly appealing for DDS to reduce the injected dose of drugs and to overcome the lack of specificity and selectivity for the ROI. It also prevents the therapeutic agent(s) from having cytotoxic effects on healthy cells. Active targeting is key to optimizing the intracellular uptake of an API by the desired target. Applying local treatment is a strategy mainly developed to enhance the bioavailability of APIs by reaching not only targeted cells but also the nucleus of cells to carry out intracellular delivery. To predetermine the biodistribution and guarantee the internalization of an API, NPs must be functionalized with targeting moieties capable of interacting with specific receptors overexpressed in the ROI to help cell penetration. Classic FDA-approved targeting moieties that are used to promote localized accumulation of NPs serving as a DDS are summarized in Table V:

The stealth property is obviously still required, even in the case of active targeting, because the gradual accumulation at a

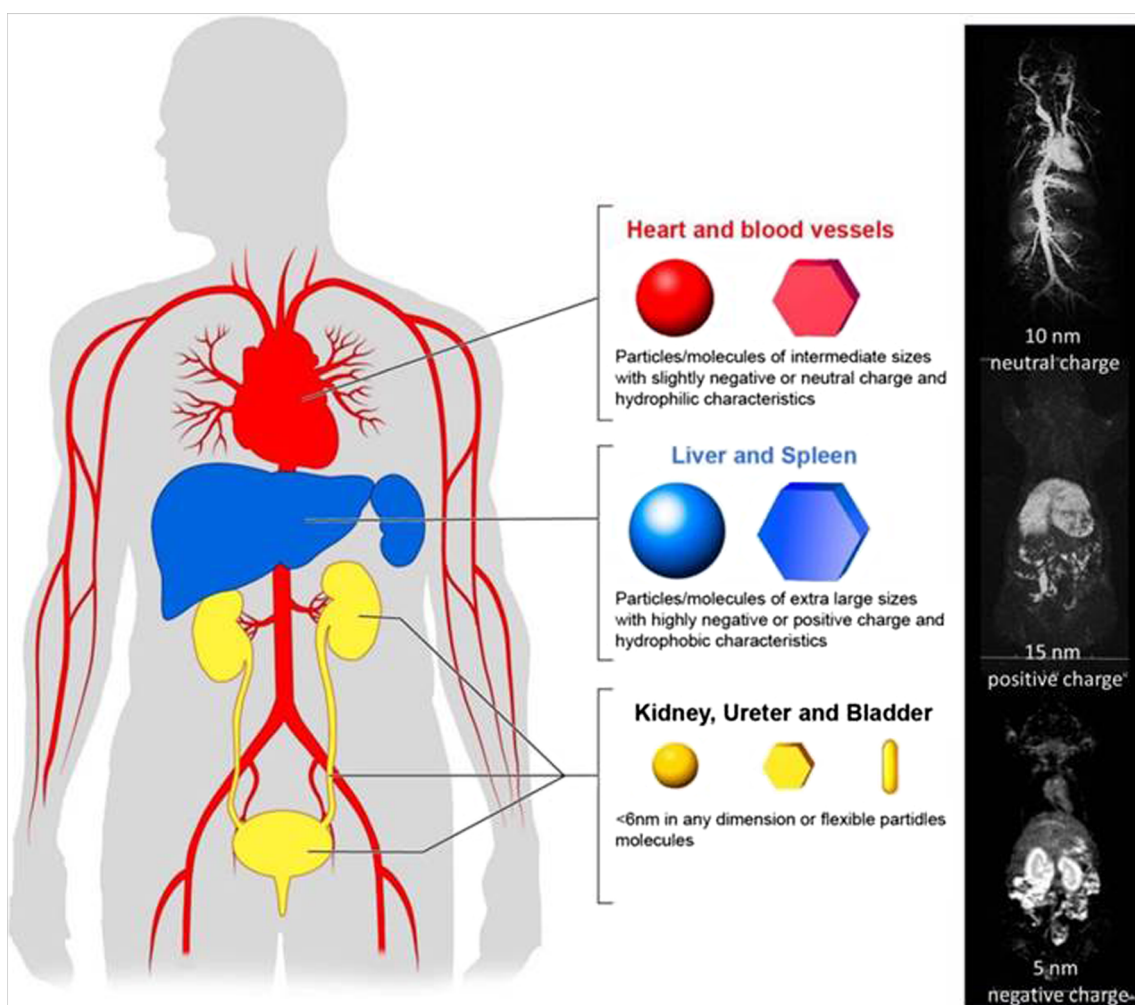


**Fig. 15** Classic pharmacokinetic profile of NPs depending on their size and their surface (reproduced with permission from [90]).

**Table V** Classical Targeting Moieties Conjugated Onto the NP Surface

Class	Ligand (marketed formulation)	Target	Reference
Antibody	Anti-HER2 (Herceptin®)	Human epidermal growth factor receptor 2 (HER2) from breast, ovarian, gastric, and prostate cancer cells	[132]
	Rituximab, anti-CD20 (Rituxan®)	CD20 antigen on malignant B-cells from lymphoma	[133, 134]
Aptamers	Anti-VEGF (Pegaptanib®), DNA, RNA	Vascular endothelial growth factor (VEGF), antigens on cancer cells	[135–138]
Protein	Transferrin	Brain parenchyma (blood-brain barrier crossing), various cancer cells	[139–142]
Peptide	Cecropin A (antimicrobial peptides), Antennapedia (cell-penetrating peptides), RGD, NGR	Cell membrane (pore forming for apoptosis ending), intracellular matrix, $\alpha_v\beta_3$ integrin receptor on tumor cells	[143, 144]
Vitamin	Folic acid	Folate receptor to reach intracellular matrix	[145, 146]

given biological site can be achieved only by giving the NPs time to circulate, reach their target and interact via specific affinities. Binding with a target may be achieved by attaching targeting agents such as ligands conjugated by covalent or electrostatic bonds with the NP surface. Programming API release is also possible by incorporating stimuli-responsive ligands such as pH-sensitive and thermosensitive macromolecules or those sensitive to the ROI microenvironment [110, 114, 117, 119, 127].

Many of these ligands are used to target cancer cells. Tumors are quite interesting tissues with complex structures having heterogeneous compartments, such as necrotic zones, densely vascularized regions, vessels with tortuosity, hemorrhage issues, and nontransformed and malignant cells [147, 148]. For a long time, tumor targeting was based on the defective vascular architecture, causing NP permeation inside the tumor microenvironment. The endothelial lining is indeed much more permeable than healthy tissue due to an endothelium pore size of 200–600 nm; thus, NPs are easily engulfed by extravasation. This high permeability is described as the enhanced permeability and retention (EPR) effect. The EPR effect promotes effective meetings between NPs and cellular targets, but it does not improve cellular uptake or specific interactions. The “leaky” blood vessels are in fact an advantageous defect to deliver NPs into the tumor microenvironment; in addition, the dysfunctional and impaired lymphatic drainage guarantees their retention in interstitial space upon transport through the endothelial lining. However, to achieve internalization, NPs must have targeting moieties to improve the bioavailability of the API to cells and, if necessary, to the inside of cells. Because of the lack of diffusion of API-loaded NPs, targeting is required. Furthermore, some drugs are very difficult to drive into cells and may induce the so-called phenomenon of multiple-drug resistance, causing some treatments to fail in patients. The development of NPs may consequently overcome this problem by trapping the API in their core and releasing it once the tumor microenvironment is reached [114, 116, 149]. Figure 16 describes how NPs improve the permeation of an API for cancer therapy.

### Toxicity

The in vivo fate of NPs includes considerations about the toxicity of NPs (composition, metabolites, interaction with physiological media, impairment of biological entities and/or functions) and their composition, and degradation products once metabolism occurs. Nanotoxicity is an emerging field, but since nanomedicine is increasingly used, there is a real need to understand how long-term retention of NPs and/or their degradation might impair the functionality of the human body [76, 114].

To conclude, it seems that NPs dedicated to biomedical uses should exhibit stringent properties to prevent adverse effects on health once in contact with biological tissues, fluids and entities. For use as an imaging CA, NPs should also be loaded with CAs and be as safe and efficient as possible. Their versatility is a valuable asset and makes them quite appealing nanovehicles as well as imaging CAs rather than a platform for real-time monitoring of treatment.

The optimum nanoparticulate CA should therefore fulfill the following specifications: first, regarding the physicochemical characteristics and composition, the CA must be i) made of biocompatible components easily formulated into nontoxic nanoparticulate systems. Colloids should be composed of ii-1) a core-shell assembly based on ii-2) a protective shield with a PEGylated hairy shell to provide stealth properties and a steric barrier against aggregation and to prevent the inner part of the assembly from leaking by efficient encapsulation or trapping of the inner materials and ii-3) a cargo with API(s) as the core. For imaging purposes, the core must exhibit very high contrast enhancement ability by means of a high payload of contrasting materials to reduce the administered dose and avoid possible side effects. The design should include iii) a neutral and hydrophilic surface because of PEG and a narrow size distribution (between 50 nm and 200 nm as the mean diameter) to avoid embolism and premature clearance by fooling the immune system, and to promote colloidal stability, the system should feature prolonged circulation time in the blood pool and homogenous biodistribution and accumulation. The surface may also be functionalized for iv)

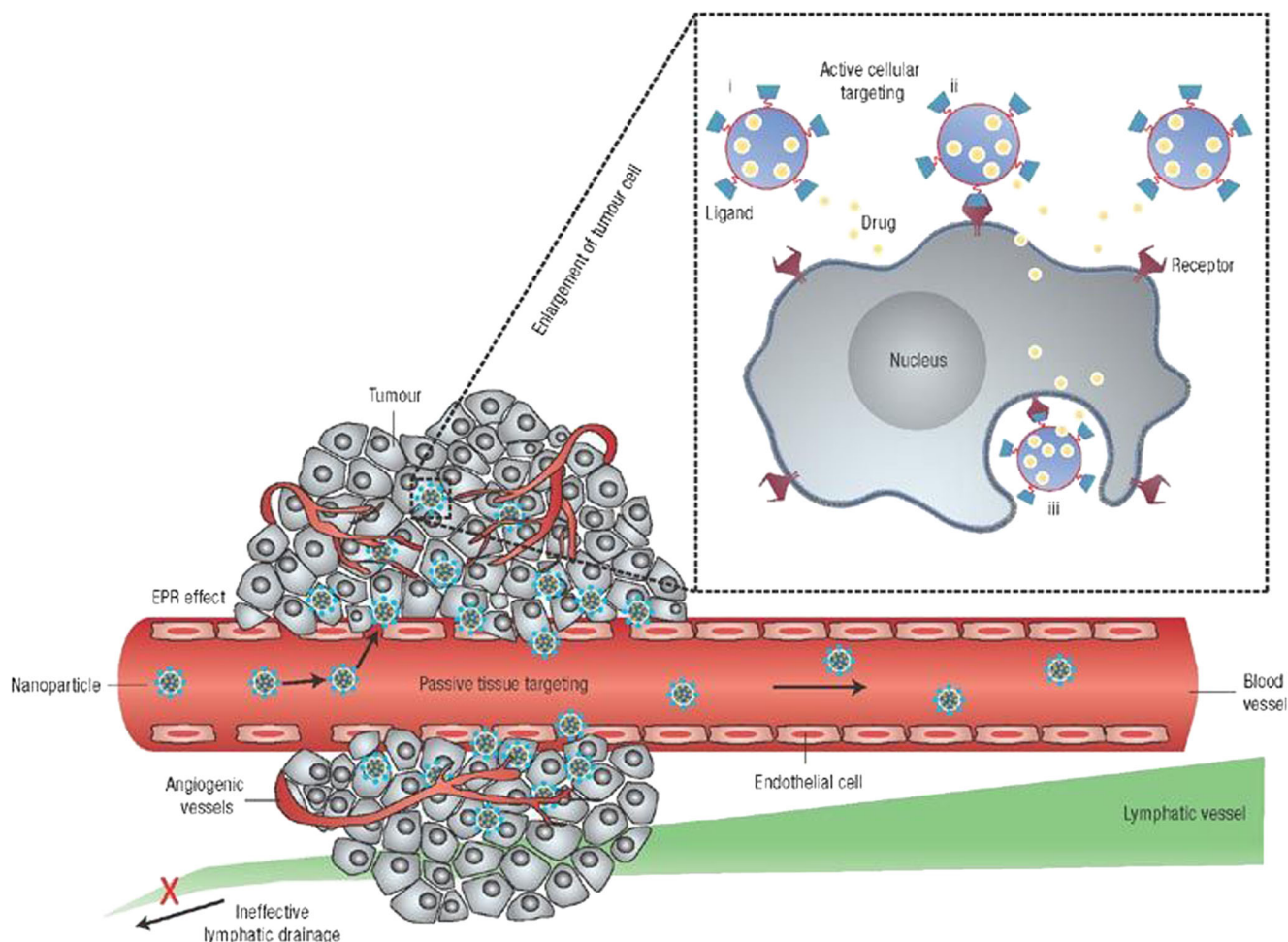


**Fig. 16** Schematic representation of passive and active targeting mechanisms to deliver API-loaded NPs to tumors. Passive tissue targeting is achieved by extravasation of NPs through the EPR effect. Active cellular targeting is achieved by functionalization of the NP surface to promote cell-specific recognition and binding. Three delivery pathways of the NP payload are depicted: i) near the target cells, ii) at the extracellular level after attachment onto the cell membrane and iii) upon cellular uptake of the NPs (adapted from [119]).

vectorization needs towards targeting the ROI and the associated cells and/or intracellular matrix with active targeting moieties able to bind with overexpressed receptors on the target surface. v-1) The pharmacokinetics and biodistribution should be programmed in order to v-2) ensure localized accumulation to concentrate the probe and to v-3) avoid administration of NPs-based CA with unpredictable degradation leading to harmful breakdown product(s).

Regarding the properties required to be considered as an upgraded kind of multifunctional CA, NPs should have intrinsic advantages for translation to the clinical scale: they have offer vi) good solubilization of drugs within their core, vii) protection of the API against degradation through encapsulation as a hermetic assembly, viii) controlled release of a therapeutic-based API to reduce cytotoxicity to nontargeted tissue and, ix) if necessary, improve intracellular uptake and enhance bioavailability. Figure 17 collects the main features of a multifunctional probe based on a nanoparticulate system for tumor imaging and therapy.

## Overview of Types of NPs and NCs for Biomedical Applications

A wide range of NPs are currently described in the literature. They can be composed of organic, inorganic, hybrid, rigid or flexible materials. As mentioned before for MRI CAs,  $Gd^{3+}$  chelates and SPIONs are already applied in the clinic and are based on a nanoscale structure, which means that some inorganic NPs and/or nanoassemblies involving an inorganic core and organic shell are on the market. It should be mentioned that the core-shell structure can also be an inorganic-inorganic assembly with a metallic coating [150, 151] or a nanocomposite with, for example, a silica shell [95, 152] and carbon coating [153]. An increasing number of NPs investigated are based on NC systems with inner and outer parts. These NCs are generally based on a lipid-based structure and are appealing owing to their high biocompatibility (nontoxic and chemically stable components, stable in physiological media, inert to tissue), high loading capacity of API(s), easy formulation, tailorable surface for applying any kind

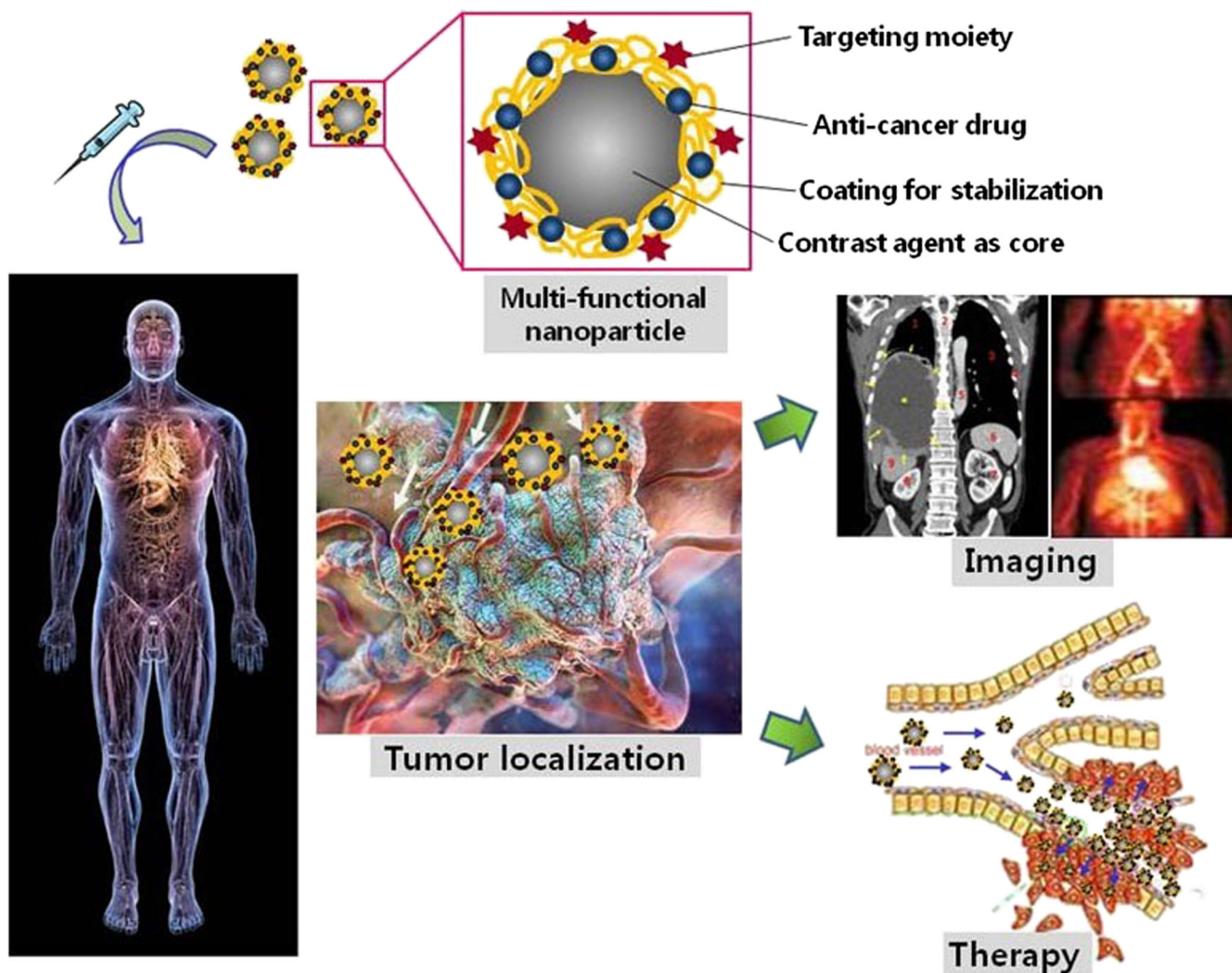


**Fig. 17** Schematic representation of optimum NPs used for biomedical application (reproduced with permission from [118]).

of targeting strategy, and improved biodistribution and pharmacokinetic profile. Considering the aforementioned advantages, these NCs offer a great alternative to iodine-based molecules used as CAs for X-ray imaging as well as excellent potential as nanovehicles for stabilizing inorganic compounds used for MRI contrast enhancement [1, 50, 96, 110]. The general inventory of lipid-based NCs allows researchers to rely on the following carriers as colloidal CAs for MRI and X-ray imaging: liposomes (LPs), dendrimers (DEs), nanoemulsions (NEs), polymeric macromolecule-based carriers or polymeric NPs (PNPs) (micelles, nanospheres and nanocapsules), and lipoproteins (LPP) [1, 20, 30, 33, 49, 50, 96, 154, 155]. Descriptions and several examples of each NC used to drive CAs in vivo are presented hereinafter. Interestingly, many novel types of nanoparticles are still constantly under development by research teams and are mainly tailored to applied needs in collaboration with clinicians. For instance, in the case of X-ray imaging, there are recent examples of the visualization of the pulmonary vasculature for minimally invasive thoracic surgery planning by using a liposomal formulation [156], active targeting of lung cancer through

antibody-decorated gold NPs [157], or fine detection tumor imaging [91, 158]. For MRI or multimodal CT/MRI, the same trend is followed through the development of CAs with enhanced imaging properties [159] aiming, for instance, to target macrophages for treating breast cancer [160], the brain [161], or aortic wall inflammation [162].

### Liposomes

Long-time circulating LPs are based on spherical vesicular self-assembling PEGylated phospholipids enclosing an aqueous core and a lipid bilayer. Hydrophilic and lipophilic API(s) can be encapsulated either within the inner core or the outer lipid membrane, respectively. A common technique to produce LPs is the ultrasonication method. They constitute one of the oldest NCs used as a DDS. Tremendous progress was made to extend their circulating time by surface functionalization with stealth polymers such as PEG. As shown in Fig. 18, similar to SPIONS and gadolinium-based compounds (magnetoliposomes), they were used often as stabilizing carriers of inorganic CAs rather

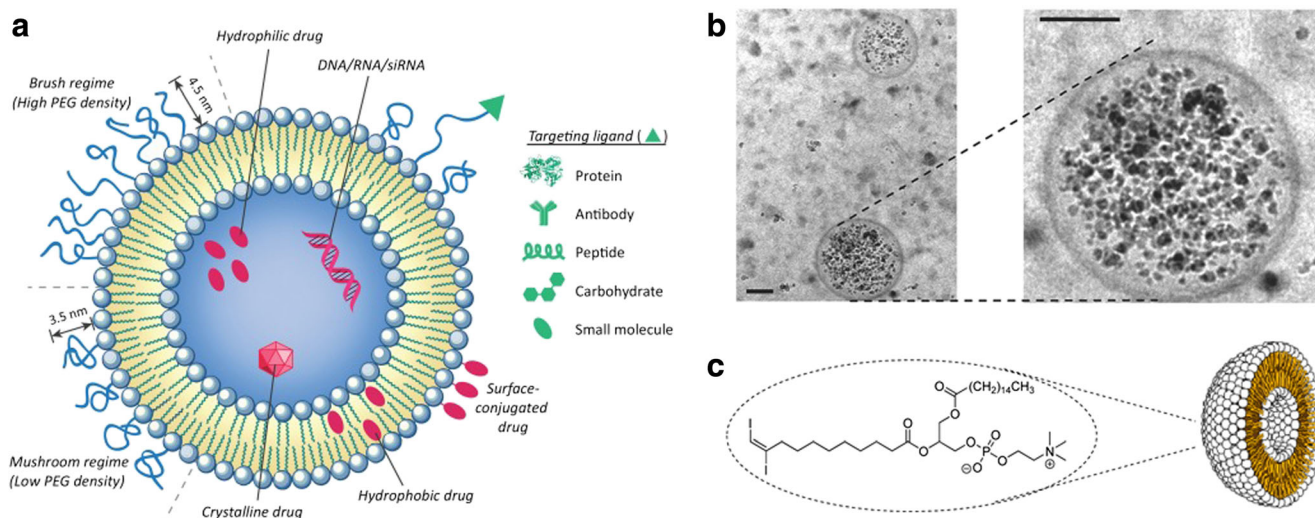


**Fig. 18** (a) Various features in the form of a multifunctional LP used as a targeted DDS (reproduced with permission from [127]). (b) TEM micrograph of magnetoliposomes based on SPION-loaded LPs for T2-weighted MRI (black bars represent 100 nm) (reproduced with permission from [164]). (c) Chemical structure of iodinated phospholipids involved in the lipid bilayer of iodoliposomes for X-ray imaging (reproduced with permission from [20]).

than convective transporters of iodinated compounds (iodoliposomes, iodine-containing LPs) for imaging purposes. Their extreme versatility makes them promising multifunctional NCs [118, 127, 163].

### Dendrimers

DEs are perfect structured assemblies based on branched molecules with a globular shape. DEs have a three-part topology: i) an inner core that traps or anchors a single element or a group, ii) a multilayer made of repeating units, called generations, and iii) an outer surface with peripheral functions directed outward and available for functionalization. Three main pathways of preparation are provided in the literature: convergent, divergent and “click” chemistry methods. DEs have been frequently employed to carry SPIONs, T1-weighted CAs based on gadolinium derivatives (magnetodendrimers) and inorganic NPs such as gold NPs for X-ray imaging [146, 165]. DEs, such as poly(amidoamine) (PAMAM) DEs, were extensively investigated as a DDS for treatment of the GI tract by oral administration (Fig. 19) [31, 72, 117, 166, 167].

### Nanoemulsions

NEs are submicron-sized emulsified droplets, commonly oil-in-water suspensions, with sizes between 20 and 200 nm. In fact, these structures are thermodynamically stable isotropic systems made of a mixture of immiscible liquids forming a single phase by means of surfactant macromolecules. Two main processes are applied to obtain NEs: low-energy (spontaneous emulsification) and high-energy (ultrasonication, microfluidic) processes [168–172]. They offer excellent NC properties for multiple API loading, most often for imaging purposes rather than for

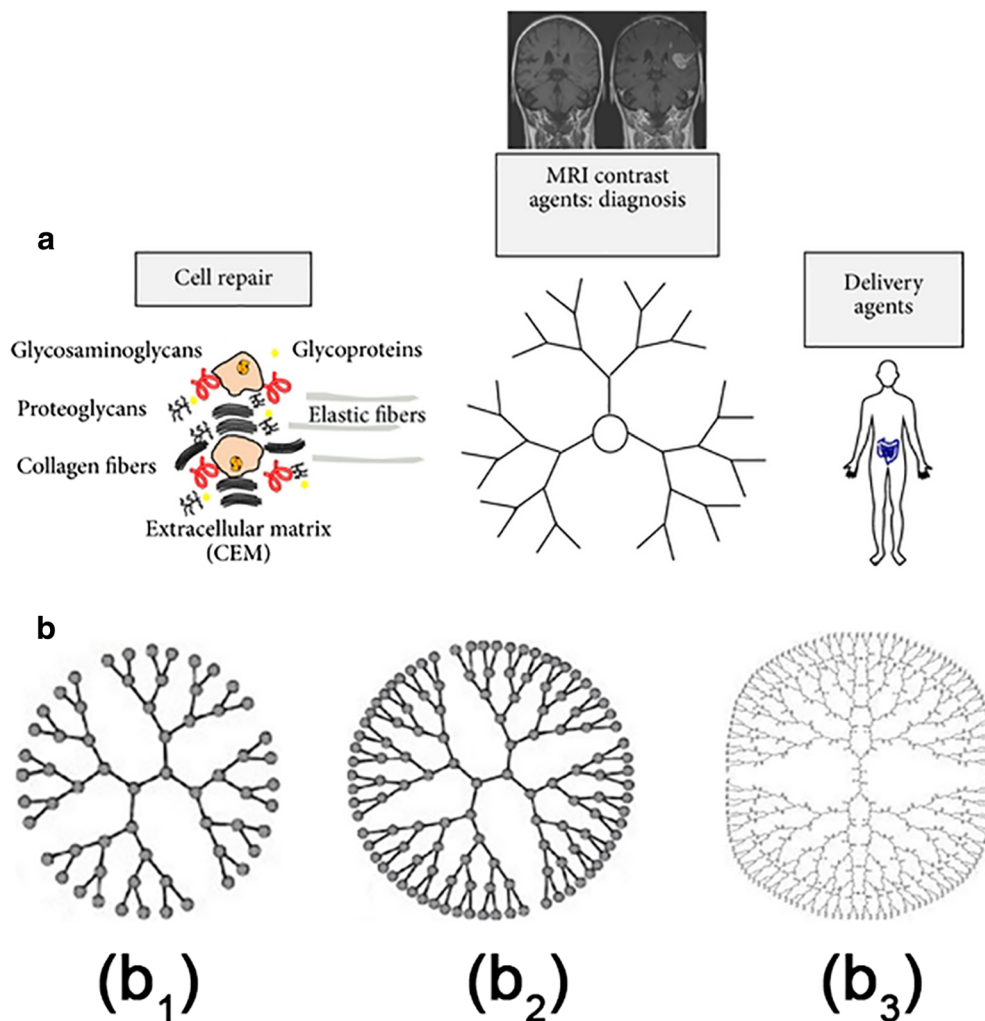
therapy. For instance, as depicted in Fig. 20, iodinated NEs were produced for liver and spleen X-ray imaging [173–175], and bimodal NEs used as MRI/optical CAs that showed efficient accumulation by the EPR were described for xenograft cancer targeting via all imaging modalities [176].

### Polymeric NCs

This family of NCs comprises a broad group that includes several types of PNPs with their own designs based on polymeric macromolecules (Fig. 21(a and b)) with amphiphilic properties. It encompasses polymeric micelles, nanocapsules and nanospheres.

Micelles are surfactant macromolecule assemblies; block copolymers are mostly used and need to be introduced above the so-called critical micellar concentration (CMC) to yield micelles. With a hydrophobic core, they can be loaded with only lipophilic API(s). Targeted PEGylated polymeric micelles were thus applied as a theranostic platform with SPIONs and doxorubicin coloaded for drug delivery to cancer cells and MRI monitoring [178]. PEGylated micelles were also investigated as vehicles of different CAs for X-ray, MRI and  $\gamma$ -ray imaging, such as for blood-pool and liver imaging [129, 179]. However, their outer part, corresponding to the hydrophilic parts of the surfactant, can be a stimuli-responsive block to promote controlled drug release under specific conditions (pH, temperature, redox, external conditions) [180–182]. Polymer-based NCs can be formulated as nanospheres and nanocapsules. The former design is a rigid construct with an insoluble polymeric matrix as a core; the corona shell is mostly a polymer providing stealth properties. API(s) can be directly grafted onto the polymer backbone, attached onto the surface or embedded within the matrix. In the case of nanocapsules, the inner core is a liquid phase

**Fig. 19** (a) Fields of biomedical applications of DEs. (b) PANAM DEs with (b<sub>1</sub>) 3, (b<sub>2</sub>) 4 and (b<sub>3</sub>) 5 generations (reproduced with permission from [167]).



surrounded by a rigid crosslinked polymeric membrane formed by cross-linking (such as Pluronic®/PEG nanocapsules [183]). Such NCs are usually employed for drug encapsulation [181–188]. Many iodinated polymers were investigated for X-ray imaging [189, 190]. Nanospheres were also used to embed SPIONs for MRI [191] (Fig. 21c) as well as for bimodal imaging with X-ray/MRI [87, 192]. Hybrids with polymers, SPIONs and gold NPs were also reported; in such cases, the SPIONs and gold NPs were not embedded in a polymeric matrix but rather were coated to yield a nanocomposite design with very good magnetic and radiopaque properties for MRI [193, 194].

### Lipoproteins

LPPs are naturally inspired NPs based on a lipid-protein system made of a phospholipid inner part for a hydrophobic payload and proteins as an outer corona layer. Natural endogenous LPPs can be low-density (LDL) (18–25 nm) or high-density (HDL) (5–12 nm) types of LPPs and can transport poorly water-soluble compounds such as lipids and

cholesterol through the bloodstream. Chylomicrons and very low density LPPs (VLDL) are also biological LPPs involved in lipid transportation. Chylomicrons are the largest LPPs with a mean size of approximately 1000 nm. VLDLs are produced by the liver and may be turned into LDL. The study of LPPs was a huge breakthrough for the understanding of cholesterol metabolism. Their differences in mean diameter and composition (Fig. 22a) cause LDL and HDL to have specific pharmacokinetic profiles: LDLs are suited for cancer targeting, whereas HDLs are more suitable to access limited access areas, such as endothelial lining and underlying tissue. HDLs have been identified as promising for cancer cell uptake [195, 196]. Both LPPs were already used for CA encapsulation, such as X-ray and fluorescence imaging via gold NP-loaded LDLs with dye-labeled surfaces. They were also used in a magnetically driven anticancer drug-loaded HDL-based DDS for T<sub>2</sub>-weighted MRI, as illustrated in Fig. 22(b and c) [197, 198]. Cormode *et al.* [199] also showed that HDLs were an outstanding nanoscale imaging platform for improved visualization of atherosclerosis and cancer-related processes.



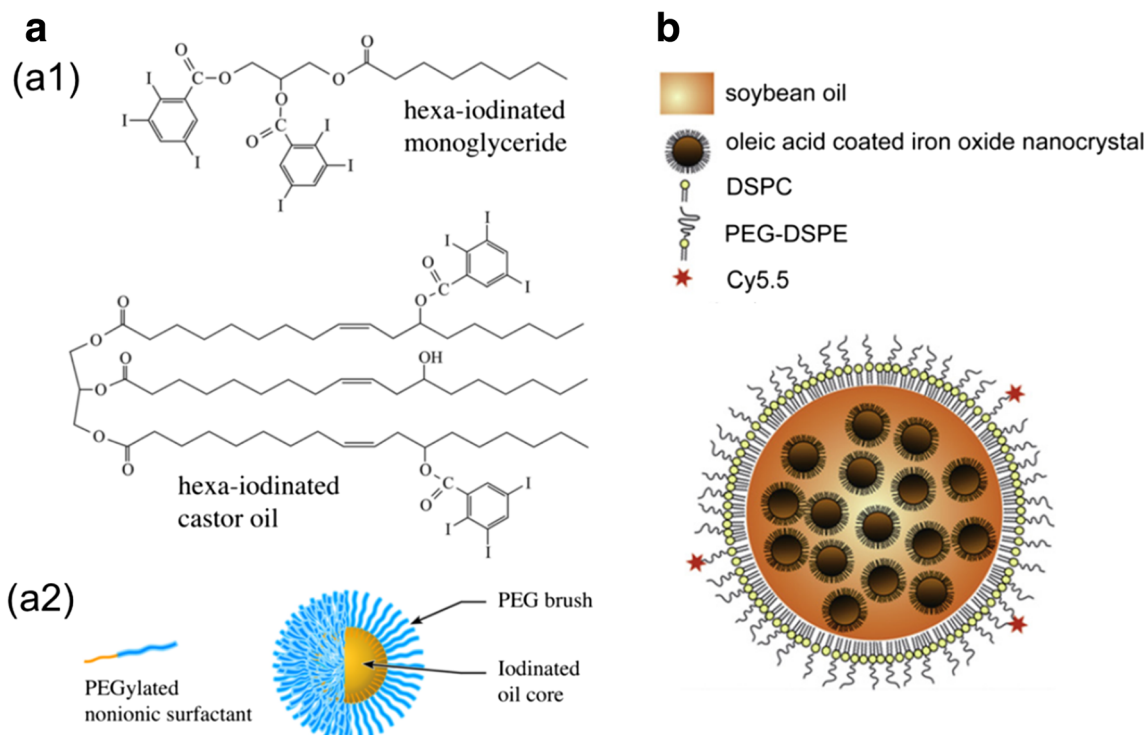


**Fig. 20** (a) Examples of (a1) iodinated oils formulated into NEs and (a2) schematic representation of iodinated nanodroplets (reproduced with permission from [175]). (b) Dual-modal NE droplet for use as a T2-weighted MRI and optical imaging contrast enhancer probe including iron oxide in its core and cyanine 5.5 (Cy5.5) as both a fluorescent dye and decorating moiety (reproduced with permission from [176]).

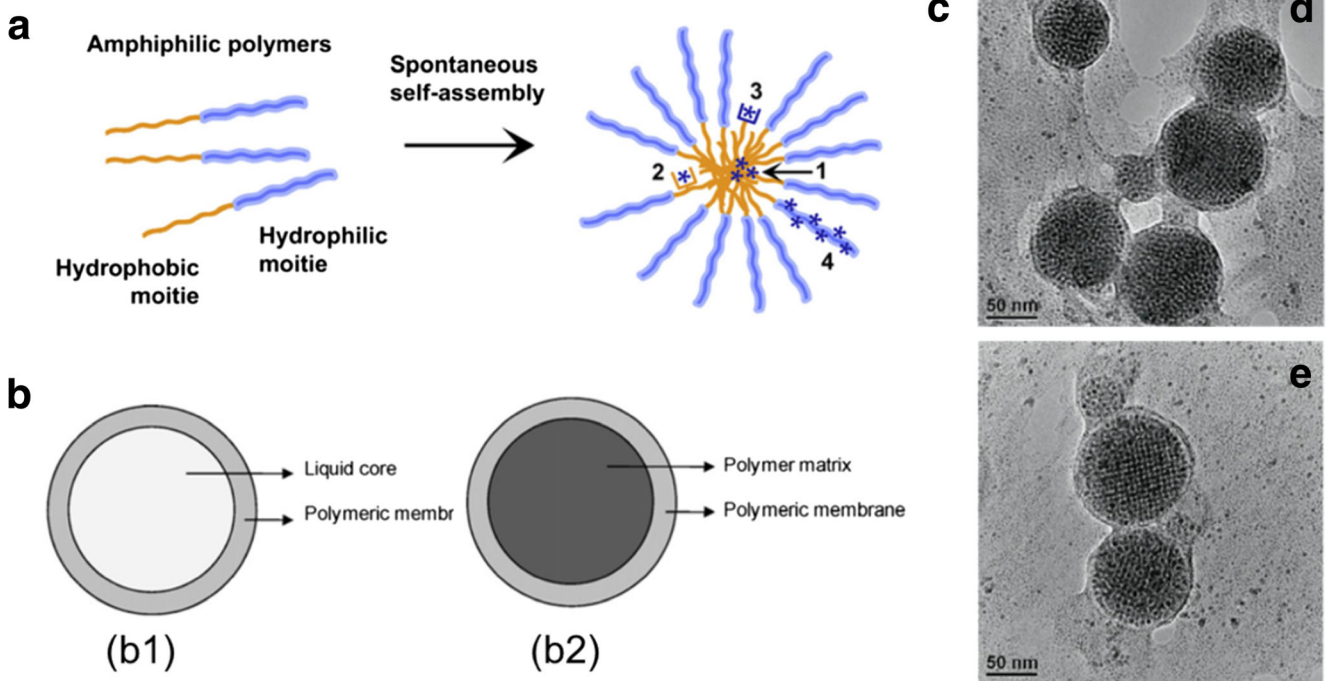


**Fig. 21** (a) Polymeric micelles self-assembling to yield micelles with (blue star) an API (1) solubilized inside the core, (2) linked to lipophilic moieties, (3) covalently conjugated to lipophilic moieties and (4) linked to hydrophilic moieties (reproduced with permission from [30]). (b) PNPs designed as (b1) nanocapsules and (b2) nanospheres. (c) Fe<sub>3</sub>O<sub>4</sub>/PMMA nanocomposite TEM micrographs (reproduced with permission from [177]).

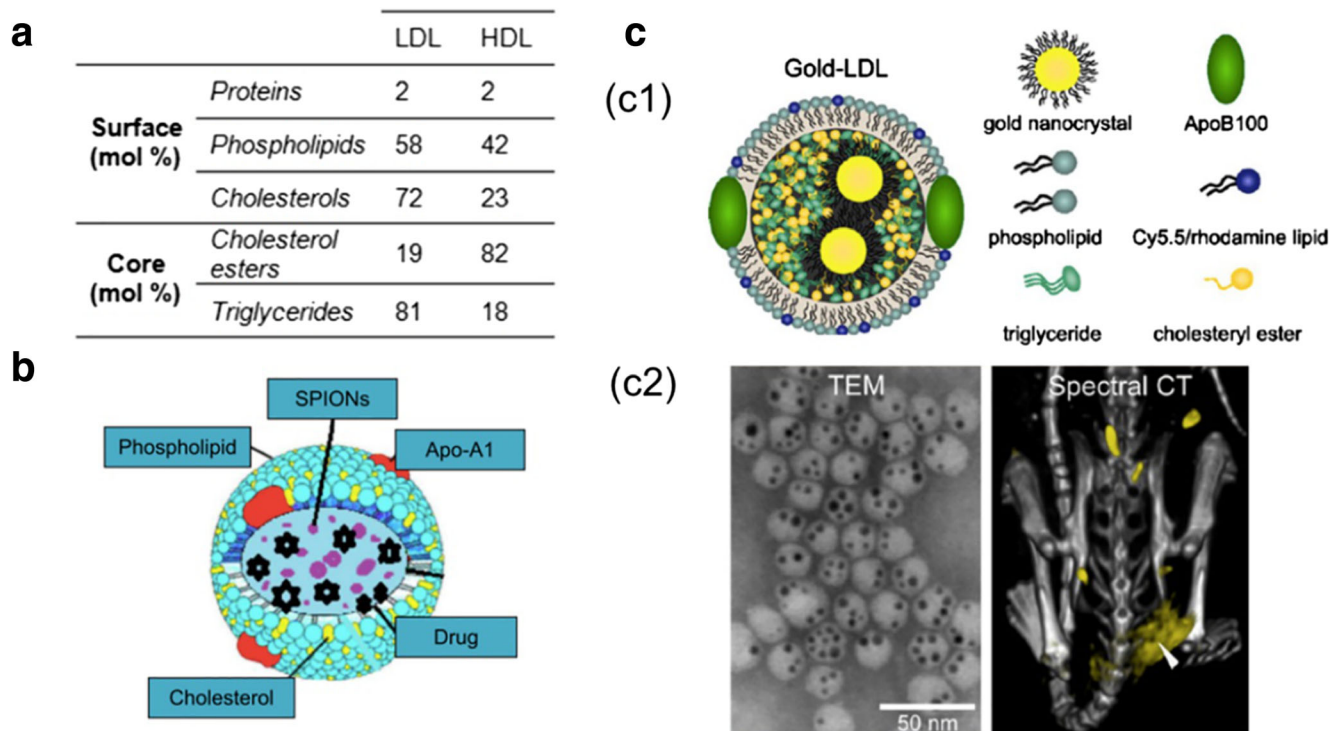


**Fig. 22** (a) Composition of LDL and HDL. (b) Schematic representation of a multifunctional HDL theranostic probe containing SPIONs for MRI T2-weight contrast enhancement and valrubicin as an anticancer drug. (c) (c1) Schematic structure of radiopaque gold NP-labeled LDL with fluorescent dyes on the surface, (c2) (Left) TEM micrograph and (right) in vivo X-ray investigation of the tumor mouse model after administration of these bimodal LDL probes (reproduced with permission from [197, 199]).

Since all the NCs previously described have already been employed to transport either contrasting and therapeutic agents, determining the best NCs for a specific application requires review of their inherent advantages and limitations, which are provided in Table VI:

## CONCLUSION

An overview of the main imaging techniques was presented. Considering their characteristics, it appears that X-ray scanner

and MRI were the two most popular instruments for noninvasive diagnosis purposes. Huge developments have led them to the top of their capacities to yield high resolution images with complementary data. Therefore, organ, lesion, interstitial fluid and skeletal imaging are feasible without any depth penetration limit. Additionally, contrast-enhancing agents are being optimized and are moving forward towards nanotechnology to cope with the adverse effects and limitations of current blood-pool probes. Novel and appealing contrast-enhancing formulations are consequently introduced to the clinic owing to extensive research at the preclinical stages. NPs and NCs thus represent a wide family

**Table VI** Advantages and Drawbacks of Typical Lipid-Based NCs Dedicated as DDS and CA Carriers

NCs	Advantages	Limitations
LPs	Biocompatible, biodegradable, very versatile (multifunctionality, tailorable)	API leakage from aqueous core, low stability, difficult purification
DEs	Well-structured, high anchoring ability, biocompatible, stable	Low yield for large DE production, expensive to produce, elimination routes still unclear
NEs	Stable over several months, improves the pharmacokinetics of poorly water-soluble compounds, biodegradable, high payload capacity	Ostwald ripening destabilization, high amount of surfactant, expensive to produce
Micelles	High loading capacity, stimuli-responsive, spontaneous formation upon reaching the CMC, cost-effective production	Disassembly upon dilution, fast drug release
Nanospheres, Nanocapsules	Inert to biological tissues, easy to prepare, loading of various compounds, no leakage	Not always made of biodegradable polymer, aggregation, lack of knowledge about their in vivo fate
LPPs	Biocompatibility, mimicking natural biological entity, coloaded, low toxicity	Loading of hydrophobic compounds, limited number of formulation techniques, difficult purification process

of nanovehicles of APIs. These smart and multifunctional colloids are becoming the next generation of probes for all imaging instruments. Their versatile designs are key to extending beyond current limits and further into the field of theranostics and nanomedicine.

## ACKNOWLEDGMENTS AND DISCLOSURES

The authors declare that they have no conflict of interest.

## REFERENCES

- Hahn MA, Singh AK, Sharma P, Brown SC, Moudgil BM. Nanoparticles as contrast agents for *in-vivo* bioimaging: current status and future perspectives. *Anal Bioanal Chem*. 2011;399(1):3–27.
- Key J, Leary JF. Nanoparticles for multimodal *in vivo* imaging in nanomedicine. *Int J Nanomedicine*. 2014;9:711–26.
- Li X, Anton N, Zuber G, Vandamme T. Contrast agents for preclinical targeted X-ray imaging. *Adv Drug Deliv Rev*. 2014;76:116–33.
- Elsabahy M, Heo GS, Lim SM, Sun G, Wooley KL. Polymeric nanostructures for imaging and therapy. *Chem Rev*. 2015;115(19):10967–1011.
- Fass L. Imaging and cancer: a review. *Mol Oncol*. 2008;2(2):115–52.
- James ML, Gambhir SS. A molecular imaging primer: modalities, imaging agents, and applications. *Physiol Rev*. 2012;92(2):897–965.
- Koo V, Hamilton PW, Williamson K. Non-invasive *in vivo* imaging in small animal research. *Cell Oncol*. 2006;28(4):127–39.
- van der Vaart MG, Meerwaldt R, Slart RH, van Dam GM, Tio RA, Zeebregts CJ. Application of PET/SPECT imaging in vascular disease. *Eur J Vasc Endovasc Surg*. 2008;35(5):507–13.
- Huang Q, Zeng Z. A review on real-time 3D ultrasound imaging technology. *Biomed Res Int*. 2017;2017:6027029.
- Deshpande N, Needles A, Willmann JK. Molecular ultrasound imaging: current status and future directions. *Clin Radiol*. 2010;65(7):567–81.
- Michalet X, Pinaud FF, Bentolila LA, Tsay JM, Doose S, Li JJ, et al. Quantum dots for live cells, *in vivo* imaging, and diagnostics. *Science*. 2005;307(5709):538–44.
- Volkov Y. Quantum dots in nanomedicine: recent trends, advances and unresolved issues. *Biochem Biophys Res Commun*. 2015;468(3):419–27.
- He X, Ma N. An overview of recent advances in quantum dots for biomedical applications. *Colloids Surf B Biointerfaces*. 2014;124:118–31.
- Martelli C, Dico AL, Diceglie C, Lucignani G, Ottobrini L. Optical imaging probes in oncology. *Oncotarget*. 2016;7(30):48753–87.
- Bouchaala R, Mercier L, Andreiuk B, Mely Y, Vandamme T, Anton N, et al. Integrity of lipid nanocarriers in bloodstream and tumor quantified by near-infrared ratiometric FRET imaging in living mice. *J Control Release*. 2016;236:57–67.
- Kilin VN, Anton H, Anton N, Steed E, Vermot J, Vandamme TF, et al. Counterion-enhanced cyanine dye loading into lipid nano-droplets for single-particle tracking in zebrafish. *Biomaterials*. 2014;35(18):4950–7.
- Klymchenko AS, Roger E, Anton N, Anton H, Shulov I, Vermot J, et al. Highly lipophilic fluorescent dyes in nano-emulsions: towards bright non-leaking nano-droplets. *RSC Adv*. 2012;2(31):11876–86.
- Wu C, Gleysteen J, Teraphongphom NT, Li Y, Rosenthal E. *In-vivo* optical imaging in head and neck oncology: basic principles, clinical applications and future directions. *Int J Oral Sci*. 2018;10(2):10.
- Wang C, Wang Z, Zhao T, Li Y, Huang G, Sumer BD, et al. Optical molecular imaging for tumor detection and image-guided surgery. *Biomaterials*. 2018;157:62–75.
- Lusic H, Grinstaff MW. X-ray-computed tomography contrast agents. *Chem Rev*. 2013;113(3):1641–66.
- Noone TC, Semelka RC, Chaney DM, Reinhold C. Abdominal imaging studies: comparison of diagnostic accuracies resulting from ultrasound, computed tomography, and magnetic resonance imaging in the same individual. *Magn Reson Imaging*. 2004;22(1):19–24.
- Oliva MR, Saini S. Liver cancer imaging: role of CT, MRI, US and PET. *Cancer Imaging*. 2004;4:S42–6.
- Semelka RC, Martin DR, Balci C, Lance T. Focal liver lesions: comparison of dual-phase CT and multisequence multiplanar MR imaging including dynamic gadolinium enhancement. *J Magn Reson Imaging*. 2001;13(3):397–401.
- Elstob A, Gonsalves M, Patel U. Diagnostic modalities. *Int J Surg*. 2016;36:504–12.
- Elias J, Semelka RC, Altun E, Tsurusaki M, Pamuklar E, Zapparoli M, et al. Pancreatic cancer: correlation of MR findings, clinical features, and tumor grade. *J Magn Reson Imaging*. 2007;26(6):1556–63.
- Casciato M, editor. Cuatro Europeos en Chandigarh. LC+Pierre Jeanneret, Jane Drew & Maxwell Fry. *RA Rev Arquit*. 2010;12:17–24.
- Rontgen WC. On a new kind of rays. *Science*. 1896;3(59):227–31.
- Leung S. Treatment of pediatric genitourinary malignancy with interstitial brachytherapy: Peter MacCallum Cancer Institute experience with four cases. *Int J Radiat Oncol Biol Phys*. 1995;31(2):393–8.
- Yu SB, Watson AD. Metal-based X-ray contrast media. *Chem Rev*. 1999;99(9):2353–78.
- Hallouard F, Anton N, Choquet P, Constantinesco A, Vandamme T. Iodinated blood pool contrast media for preclinical X-ray imaging applications—a review. *Biomaterials*. 2010;31(24):6249–68.
- Jakhmola A, Anton N, Vandamme TF. Inorganic nanoparticles based contrast agents for X-ray computed tomography. *Adv Healthc Mater*. 2012;1(4):413–31.
- Cormode DP, Naha PC, Fayad ZA. Nanoparticle contrast agents for computed tomography: a focus on micelles. *Contrast Media Mol Imaging*. 2014;9(1):37–52.
- Lee N, Choi SH, Hyeon T. Nano-sized CT contrast agents. *Adv Mater*. 2013;25(19):2641–60.
- De La Vega JC, Hafeli UO. Utilization of nanoparticles as X-ray contrast agents for diagnostic imaging applications. *Contrast Media Mol Imaging*. 2015;10(2):81–95.
- Badea CT, Drangova M, Holdsworth DW, Johnson GA. *In vivo* small-animal imaging using micro-CT and digital subtraction angiography. *Phys Med Biol*. 2008;53(19):R319–50.
- Holdsworth DW, Thornton MM. Micro-CT in small animal and specimen imaging. *Trends Biotechnol*. 2002;20(8):S34–9.
- Schambach SJ, Bag S, Schilling L, Groden C, Brockmann MA. Application of micro-CT in small animal imaging. *Methods*. 2010;50(1):2–13.
- Ritman EL. Small-animal CT - its difference from, and impact on, clinical CT. *Nucl Instrum Methods Phys Res A*. 2007;580(2):968–70.

39. Brenner DJ, Hall EJ. Computed tomography—an increasing source of radiation exposure. *N Engl J Med.* 2007;357(22):2277–84.
40. Jones JG, Mills CN, Mogensen MA, Lee CI. Radiation dose from medical imaging: a primer for emergency physicians. *West J Emerg Med.* 2012;13(2):202–10.
41. Idee JM, Guiu B. Use of lipiodol as a drug-delivery system for transcatheter arterial chemoembolization of hepatocellular carcinoma: a review. *Crit Rev Oncol Hematol.* 2013;88(3):530–49.
42. Widmark JM. Imaging-related medications: a class overview. *Proc (Bayl Univ Med Cent).* 2007;20(4):408–17.
43. Suzuki H, Oshima H, Shiraki N, Ikeya C, Shibamoto Y. Comparison of two contrast materials with different iodine concentrations in enhancing the density of the the aorta, portal vein and liver at multi-detector row CT: a randomized study. *Eur Radiol.* 2004;14(11):2099–104.
44. Zagorchev L, Oses P, Zhuang ZW, Moodie K, Mulligan-Kehoe MJ, Simons M, et al. Micro computed tomography for vascular exploration. *J Angiogenes Res.* 2010;2:7.
45. Kandanapitiye MS, Gao M, Molter J, Flask CA, Huang SD. Synthesis, characterization, and X-ray attenuation properties of ultrasmall BiOI nanoparticles: toward renal clearable particulate CT contrast agents. *Inorg Chem.* 2014;53(19):10189–94.
46. Briguori C, Tavano D, Colombo A. Contrast agent—associated nephrotoxicity. *Prog Cardiovasc Dis.* 2003;45(6):493–503.
47. Bottinor W, Polkamally P, Jovin I. Adverse reactions to iodinated contrast media. *Int J Angiol.* 2013;22(3):149–54.
48. Suckow CE, Stout DB. MicroCT liver contrast agent enhancement over time, dose, and mouse strain. *Mol Imaging Biol.* 2008;10(2):114–20.
49. Anton N, Vandamme TF. Nanotechnology for computed tomography: a real potential recently disclosed. *Pharm Res.* 2014;31(1):20–34.
50. Cormode DP, Skajaa T, Fayad ZA, Mulder WJ. Nanotechnology in medical imaging: probe design and applications. *Arterioscler Thromb Vasc Biol.* 2009;29(7):992–1000.
51. McClatchy DM, Zuurbier RA, Wells WA, Paulsen KD, Pogue BW. Micro-computed tomography enables rapid surgical margin assessment during breast conserving surgery (BCS): correlation of whole BCS micro-CT readings to final histopathology. *Breast Cancer Res Treat.* 2018;172(3):587–95.
52. Qiu SQ, Dorrius MD, de Jongh SJ, Jansen L, de Vries J, Schroder CP, et al. Micro-computed tomography (micro-CT) for intraoperative surgical margin assessment of breast cancer: a feasibility study in breast conserving surgery. *Eur J Surg Oncol.* 2018;44(11):1708–13.
53. Oikonomou EK, Marwan M, Desai MY, Mancio J, Alashi A, Centeno EH, et al. Non-invasive detection of coronary inflammation using computed tomography and prediction of residual cardiovascular risk (the CRISP CT study): a post-hoc analysis of prospective outcome data. *Lancet.* 2018;392(10151):929–39.
54. O'Sullivan JDB, Behnsen J, Starborg T, MacDonald AS, Phythian-Adams AT, Else KJ, et al. X-ray micro-computed tomography (muCT): an emerging opportunity in parasite imaging. *Parasitology.* 2018;145(7):848–54.
55. Tang R, Saksena M, Coopey SB, Fernandez L, Buckley JM, Lei L, et al. Intraoperative micro-computed tomography (micro-CT): a novel method for determination of primary tumour dimensions in breast cancer specimens. *Br J Radiol.* 2016;89(1058):20150581.
56. Sun C, Lee JS, Zhang M. Magnetic nanoparticles in MR imaging and drug delivery. *Adv Drug Deliv Rev.* 2008;60(11):1252–65.
57. Mornet S, Vasseur S, Grasset F, Duguet E. Magnetic nanoparticle design for medical diagnosis and therapy. *J Mater Chem.* 2004;14(14):2161–75.
58. Laurent S, Forge D, Port M, Roch A, Robic C, Elst LV, et al. Magnetic iron oxide nanoparticles: synthesis, stabilization, vectorization, physicochemical characterizations, and biological applications. *Chem Rev.* 2008;108(6):2064–110.
59. Louis R. Hawaiian place names: mnemonic symbols in a hawaiian performance cartography. In: Paper read at Indigenous Knowledges Conference. Wellington, NZ: Rutherford House, Pipitea Campus, Victoria University; 2005. p. 167–81.
60. Tognarelli JM, Dawood M, Shariff MI, Grover VP, Crossey MM, Cox IJ, et al. Magnetic resonance spectroscopy: principles and techniques: lessons for clinicians. *J Clin Exp Hepatol.* 2015;5(4):320–8.
61. Damadian R. Tumor detection by nuclear magnetic resonance. *Science.* 1971;171(3976):1151–3.
62. Lauterbur PC. Image formation by induced local interactions: examples employing nuclear magnetic resonance. *Nature.* 1973;242(5394):190–1.
63. Garroway AN, Grannell PK, Mansfield P. Image formation in NMR by a selective irradiative process. *J Phys C Solid State Phys.* 1974;7(24):L457–62.
64. Mansfield P, Maudsley A. Medical imaging by NMR. *J Magn Reson.* 1980;27:101–19.
65. Edelstein WA, Hutchison JM, Johnson G, Redpath T. Spin warp NMR imaging and applications to human whole-body imaging. *Phys Med Biol.* 1980;25(4):751–6.
66. Hutchinson JMS, Edelstein WA, Johnson G. A whole-body NMR imaging machine. *J Physics E: Sci Instrum.* 1980;13(9):947–55.
67. Pykett IL, Rzedzian RR. Instant images of the body by magnetic resonance. *Magn Reson Med.* 1987;5(6):563–71.
68. Na HB, Song IC, Hyeon T. Inorganic nanoparticles for MRI contrast agents. *Adv Mater.* 2009;21(21):2133–48.
69. Nitz WR, Reimer P. Contrast mechanisms in MR imaging. *Eur Radiol.* 1999;9(6):1032–46.
70. Chavhan GB, Babyn PS, Thomas B, Shroff MM, Haacke EM. Principles, techniques, and applications of T2\*-based MR imaging and its special applications. *Radiographics.* 2009;29(5):1433–49.
71. Strijkers GJ, Mulder WJ, van Tilborg GA, Nicolay K. MRI contrast agents: current status and future perspectives. *Anticancer Agents Med Chem.* 2007;7(3):291–305.
72. Geraldies CF, Laurent S. Classification and basic properties of contrast agents for magnetic resonance imaging. *Contrast Media Mol Imaging.* 2009;4(1):1–23.
73. Hao D, Ai T, Goerner F, Hu X, Runge VM, Tweedle M. MRI contrast agents: basic chemistry and safety. *J Magn Reson Imaging.* 2012;36(5):1060–71.
74. Sahraei Z, Mirabzadeh M, Fadaei-Fouladi D, Eslami N, Eshraghi A. Magnetic resonance imaging contrast agents: a review of literature. *J Pharm Care.* 2014;2:177–82.
75. Chen W, Cormode DP, Fayad ZA, Mulder WJM. Nanoparticles as magnetic resonance imaging contrast agents for vascular and cardiac diseases. *Wiley Interdiscip Rev Nanomed Nanobiotechnol.* 2011;3(2):146–61.
76. Singh N, Jenkins GJ, Asadi R, Doak SH. Potential toxicity of superparamagnetic iron oxide nanoparticles (SPION). *Nano Rev.* 2010;1:5358.
77. Y-XJ W. Superparamagnetic iron oxide based MRI contrast agents: current status of clinical application. *Quant Imaging Med Surg.* 2011;1(1):35–40.
78. Wang YX. Current status of superparamagnetic iron oxide contrast agents for liver magnetic resonance imaging. *World J Gastroenterol.* 2015;21(47):13400–2.
79. Wang YX, Hussain SM, Krestin GP. Superparamagnetic iron oxide contrast agents: physicochemical characteristics and applications in MR imaging. *Eur Radiol.* 2001;11(11):2319–31.
80. Corot C, Robert P, Idee JM, Port M. Recent advances in iron oxide nanocrystal technology for medical imaging. *Adv Drug Deliv Rev.* 2006;58(14):1471–504.

81. Lodhia J, Mandarano G, Ferris N, Eu P, Cowell S. Development and use of iron oxide nanoparticles (Part 1): synthesis of iron oxide nanoparticles for MRI. *Biomed Imaging Interv J*. 2010;6(2):e12.
82. Wan J, Cai W, Meng X, Liu E. Monodisperse water-soluble magnetite nanoparticles prepared by polyol process for high-performance magnetic resonance imaging. *Chem Commun (Camb)*. 2007;4(47):5004–6.
83. Lee N, Cho HR, Oh MH, Lee SH, Kim K, Kim BH, et al. Multifunctional Fe<sub>3</sub>O<sub>4</sub>/TaO(x) core/shell nanoparticles for simultaneous magnetic resonance imaging and X-ray computed tomography. *J Am Chem Soc*. 2012;134(25):10309–12.
84. Jarzyna PA, Gianella A, Skajaa T, Knudsen G, Deddens LH, Cormode DP, et al. Multifunctional imaging nanoprobe. *Wiley Interdiscip Rev Nanomed Nanobiotechnol*. 2010;2(2):138–50.
85. Bardhan R, Chen W, Bartels M, Perez-Torres C, Botero MF, McAninch RW, et al. Tracking of multimodal therapeutic nanocomplexes targeting breast cancer *in vivo*. *Nano Lett*. 2010;10(12):4920–8.
86. Yang J, Lim EK, Lee HJ, Park J, Lee SC, Lee K, et al. Fluorescent magnetic nanohybrids as multimodal imaging agents for human epithelial cancer detection. *Biomaterials*. 2008;29(16):2548–55.
87. Hagit A, Soenke B, Johannes B, Shlomo M. Synthesis and characterization of dual modality (CT/MRI) core-shell microparticles for embolization purposes. *Biomacromolecules*. 2010;11(6):1600–7.
88. Xue S, Wang Y, Wang M, Zhang L, Du X, Gu H, et al. Iodinated oil-loaded, fluorescent mesoporous silica-coated iron oxide nanoparticles for magnetic resonance imaging/computed tomography/fluorescence trimodal imaging. *Int J Nanomedicine*. 2014;9:2527–38.
89. Ding H, Wu F. Image guided biodistribution and pharmacokinetic studies of theranostics. *Theranostics*. 2012;2(11):1040–53.
90. Kobayashi H, Watanabe R, Choyke PL. Improving conventional enhanced permeability and retention (EPR) effects; what is the appropriate target? *Theranostics*. 2013;4(1):81–9.
91. Ashton JR, Castle KD, Qi Y, Kirsch DG, West JL, Badea CT. Dual-energy CT imaging of tumor liposome delivery after gold nanoparticle-augmented radiation therapy. *Theranostics*. 2018;8(7):1782–97.
92. Barsanti C, Lenzarini F, Kusmic C. Diagnostic and prognostic utility of non-invasive imaging in diabetes management. *World J Diabetes*. 2015;6(6):792–806.
93. Senpan A, Caruthers SD, Rhee I, Mauro NA, Pan D, Hu G, et al. Conquering the dark side: colloidal iron oxide nanoparticles. *ACS Nano*. 2009;3(12):3917–26.
94. Xu L, Cheng L, Wang C, Peng R, Liu Z. Conjugated polymers for photothermal therapy of cancer. *Polym Chem*. 2014;5(5):1573–80.
95. Kumar S, Daverey A, Khalilzad-Sharghi V, Sahu NK, Kidambi S, Othman SF, et al. Theranostic fluorescent silica encapsulated magnetic nanoassemblies for *in vitro* MRI imaging and hyperthermia. *RSC Adv*. 2015;5(66):53180–8.
96. Torchilin VP. Multifunctional nanocarriers. *Adv Drug Deliv Rev*. 2012;64:302–15.
97. Bogart LK, Pourroy G, Murphy CJ, Puentes V, Pellegrino T, Rosenblum D, et al. Nanoparticles for imaging, sensing, and therapeutic intervention. *ACS Nano*. 2014;8(4):3107–22.
98. Kircher MF, Willmann JK. Molecular body imaging: MR imaging, CT, and US. part I. principles. *Radiology*. 2012;263(3):633–43.
99. Morse MD. Clusters of transition-metal atoms. *Chem Rev*. 1986;86(6):1049–109.
100. Henglein A. Small-particle research: physicochemical properties of extremely small colloidal metal and semiconductor particles. *Chem Rev*. 1989;89(8):1861–73.
101. Faraday M. The bakerian lecture: experimental relations of gold (and other metals) to light. *Philos Trans R Soc Lond*. 1857;147:145–81.
102. Goesmann H, Feldmann C. Nanoparticulate functional materials. *Angew Chem Int Ed Engl*. 2010;49(8):1362–95.
103. Issa B, Obaidat IM, Albiss BA, Haik Y. Magnetic nanoparticles: surface effects and properties related to biomedicine applications. *Int J Mol Sci*. 2013;14(11):21266–305.
104. Indira T, Lakshmi P. Magnetic nanoparticles - a review. *Int J Pharm Sci Nanotech*. 2010;3:1035–42.
105. Tartaj P, Morales MP, Gonzalez-Carreño T, Veintemillas-Verdaguer S, Bomati-Miguel O, Roca AG, et al. Biomedical applications of magnetic nanoparticles. In: KHJ B, Cahn RW, Flemings MC, Ilshner B, Kramer EJ, Mahajan S, et al., editors. *Encyclopedia of materials: science and technology*. Oxford: Elsevier; 2007. p. 1–7.
106. Tyndall J. On the blue colour of the sky, the polarization of skylight, and on the polarization of light by cloudy matter generally. *Proc R Soc Lond*. 1868;17:223–33.
107. Mie G. Beiträge zur optik trüber medien, speziell kolloidaler metallösungen. *Ann Phys*. 1908;330(3):377–445.
108. Young A. Rayleigh scattering. *Appl Opt*. 1981;20(4):533–5.
109. Gao J, Gu H, Xu B. Multifunctional magnetic nanoparticles: design, synthesis, and biomedical applications. *Acc Chem Res*. 2009;42(8):1097–107.
110. Torchilin VP. Targeted pharmaceutical nanocarriers for cancer therapy and imaging. *AAPS J*. 2007;9(2):E128–47.
111. Liang Y, Hilal N, Langston P, Starov V. Interaction forces between colloidal particles in liquid: theory and experiment. *Adv Colloid Interface Sci*. 2007;134–135:151–66.
112. Verwey E, Overbeek J, van Nes K. Theory of the stability of lyophobic colloids-the interactions of soil particles having an electrical double layer. Amsterdam: Elsevier; 1948. p. 631–6.
113. Kolhatkar AG, Jamison AC, Litvinov D, Willson RC, Lee TR. Tuning the magnetic properties of nanoparticles. *Int J Mol Sci*. 2013;14(8):15977–6009.
114. Veiseh O, Gunn JW, Zhang M. Design and fabrication of magnetic nanoparticles for targeted drug delivery and imaging. *Adv Drug Deliv Rev*. 2010;62(3):284–304.
115. Aggarwal P, Hall JB, McLeland CB, Dobrovolskaia MA, McNeil SE. Nanoparticle interaction with plasma proteins as it relates to particle biodistribution, biocompatibility and therapeutic efficacy. *Adv Drug Deliv Rev*. 2009;61(6):428–37.
116. Brigger I, Dubernet C, Couvreur P. Nanoparticles in cancer therapy and diagnosis. *Adv Drug Deliv Rev*. 2002;54(5):631–51.
117. Parveen S, Misra R, Sahoo SK. Nanoparticles: a boon to drug delivery, therapeutics, diagnostics and imaging. *Nanomedicine*. 2012;8(2):147–66.
118. Bae KH, Chung HJ, Park TG. Nanomaterials for cancer therapy and imaging. *Mol Cell*. 2011;31(4):295–302.
119. Peer D, Karp JM, Hong S, Farokhzad OC, Margalit R, Langer R. Nanocarriers as an emerging platform for cancer therapy. *Nat Nanotechnol*. 2007;2:751–60.
120. Yu M, Huang S, Yu KJ, Clyne AM. Dextran and polymer polyethylene glycol (PEG) coating reduce both 5 and 30 nm iron oxide nanoparticle cytotoxicity in 2D and 3D cell culture. *Int J Mol Sci*. 2012;13(5):5554–70.
121. Shaterabadi Z, Nabiyouni G, Soleymani M. High impact of in situ dextran coating on biocompatibility, stability and magnetic properties of iron oxide nanoparticles. *Mater Sci Eng C Mater Biol Appl*. 2017;75:947–56.
122. Kenley RA, Lee MO, Mahoney TR, Sanders LM. Poly(lactide-co-glycolide) decomposition kinetics *in vivo* and *in vitro*. *Macromolecules*. 1987;20(10):2398–403.
123. Yang YY, Chung TS, Ng NP. Morphology, drug distribution, and *in vitro* release profiles of biodegradable polymeric microspheres

- containing protein fabricated by double-emulsion solvent extraction/evaporation method. *Biomaterials*. 2001;22(3):231–41.
124. Redhead HM, Davis SS, Illum L. Drug delivery in poly(lactide-co-glycolide) nanoparticles surface modified with poloxamer 407 and poloxamine 908: *in vitro* characterisation and *in vivo* evaluation. *J Control Release*. 2001;70(3):353–63.
  125. Alvarez-Lorenzo C, Rey-Rico A, Sosnik A, Taboada P, Concheiro A. Poloxamine-based nanomaterials for drug delivery. *Front Biosci (Elite Ed)*. 2010;2:424–40.
  126. Storm G, Belliot SO, Daemen T, Lasic DD. Surface modification of nanoparticles to oppose uptake by the mononuclear phagocyte system. *Adv Drug Deliv Rev*. 1995;17(1):31–48.
  127. Noble GT, Stefanick JF, Ashley JD, Kiziltepe T, Bilgicer B. Ligand-targeted liposome design: challenges and fundamental considerations. *Trends Biotechnol*. 2014;32(1):32–45.
  128. Torchilin VP, Trubetsky VS. Which polymers can make nanoparticulate drug carriers long-circulating? *Adv Drug Deliv Rev*. 1995;16(2):141–55.
  129. Torchilin VP. PEG-based micelles as carriers of contrast agents for different imaging modalities. *Adv Drug Deliv Rev*. 2002;54(2):235–52.
  130. Huang X, Teng X, Chen D, Tang F, He J. The effect of the shape of mesoporous silica nanoparticles on cellular uptake and cell function. *Biomaterials*. 2010;31(3):438–48.
  131. Huang X, Li L, Liu T, Hao N, Liu H, Chen D, et al. The shape effect of mesoporous silica nanoparticles on biodistribution, clearance, and biocompatibility *in vivo*. *ACS Nano*. 2011;5(7):5390–9.
  132. Tai W, Mahato R, Cheng K. The role of HER2 in cancer therapy and targeted drug delivery. *J Control Release*. 2010;146(3):264–75.
  133. Anderson DR, Grillo-Lopez A, Varns C, Chambers KS, Hanna N. Targeted anti-cancer therapy using rituximab, a chimeric anti-CD20 antibody (IDEC-C2B8) in the treatment of non-Hodgkin's B-cell lymphoma. *Biochem Soc Trans*. 1997;25(2):705–8.
  134. Lim SH, Beers SA, French RR, Johnson PW, Glennie MJ, Cragg MS. Anti-CD20 monoclonal antibodies: historical and future perspectives. *Haematologica*. 2010;95(1):135–43.
  135. Ng EW, Shima DT, Calias P, Cunningham ET, Guyer DR, Adamis AP. Pegaptanib, a targeted anti-VEGF aptamer for ocular vascular disease. *Nat Rev Drug Discov*. 2006;5(2):123–32.
  136. Baek SE, Lee KH, Park YS, Oh DK, Oh S, Kim KS, et al. RNA aptamer-conjugated liposome as an efficient anticancer drug delivery vehicle targeting cancer cells *in vivo*. *J Control Release*. 2014;196:234–42.
  137. Li X, Zhao Q, Qiu L. Smart ligand: aptamer-mediated targeted delivery of chemotherapeutic drugs and siRNA for cancer therapy. *J Control Release*. 2013;171(2):152–62.
  138. Yang L, Zhang X, Ye M, Jiang J, Yang R, Fu T, et al. Aptamer-conjugated nanomaterials and their applications. *Adv Drug Deliv Rev*. 2011;63(14–15):1361–70.
  139. Clark AJ, Davis ME. Increased brain uptake of targeted nanoparticles by adding an acid-cleavable linkage between transferrin and the nanoparticle core. *Proc Natl Acad Sci U S A*. 2015;112(40):12486–91.
  140. Yuan Y, Zhang L, Cao H, Yang Y, Zheng Y, Yang X-J. A polyethylenimine-containing and transferrin-conjugated lipid nanoparticle system for antisense oligonucleotide delivery to AML. *Biomed Res Int*. 2016;2016:8.
  141. Wiley DT, Webster P, Gale A, Davis ME. Transcytosis and brain uptake of transferrin-containing nanoparticles by tuning avidity to transferrin receptor. *Proc Natl Acad Sci U S A*. 2013;110(21):8662–7.
  142. Liu K, Dai L, Li C, Liu J, Wang L, Lei J. Self-assembled targeted nanoparticles based on transferrin-modified eight-arm-polyethylene glycol-dihydroartemisinin conjugate. *Sci Rep*. 2016;6:29461.
  143. Boohaker RJ, Lee MW, Vishnubhotla P, Perez JM, Khaled AR. The use of therapeutic peptides to target and to kill cancer cells. *Curr Med Chem*. 2012;19(22):3794–804.
  144. Dijkgraaf I, Kruijtz JAW, Frielink C, Corstens FHM, Oyen WJG, Liskamp RMJ, et al.  $\alpha\beta 3$  integrin-targeting of intraperitoneally growing tumors with a radiolabeled RGD peptide. *Int J Cancer*. 2007;120(3):605–10.
  145. Jain RK. Transport of molecules, particles, and cells in solid tumors. *Annu Rev Biomed Eng*. 1999;1:241–63.
  146. Peng C, Qin J, Zhou B, Chen Q, Shen M, Zhu M, et al. Targeted tumor CT imaging using folic acid-modified PEGylated dendrimer-entrapped gold nanoparticles. *Polym Chem*. 2013;4(16):4412–24.
  147. Balkwill FR, Capasso M, Hagemann T. The tumor microenvironment at a glance. *J Cell Sci*. 2012;125(Pt 23):5591–6.
  148. Li H, Fan X, Houghton J. Tumor microenvironment: the role of the tumor stroma in cancer. *J Cell Biochem*. 2007;101(4):805–15.
  149. Maeda H. The enhanced permeability and retention (EPR) effect in tumor vasculature: the key role of tumor-selective macromolecular drug targeting. *Adv Enzym Regul*. 2001;41:189–207.
  150. Gallo J, Garcia I, Padro D, Arnáiz B, Penadés S. Water-soluble magnetic glyconanoparticles based on metal-doped ferrites coated with gold: synthesis and characterization. *J Mater Chem*. 2010;20(44):10010–20.
  151. Mandal M, Kundu S, Ghosh SK, Panigrahi S, Sau TK, Yusuf SM, et al. Magnetite nanoparticles with tunable gold or silver shell. *J Colloid Interface Sci*. 2005;286(1):187–94.
  152. Sahoo B, Devi KSP, Dutta S, Maiti TK, Pramanik P, Dhara D. Biocompatible mesoporous silica-coated superparamagnetic manganese ferrite nanoparticles for targeted drug delivery and MR imaging applications. *J Colloid Interface Sci*. 2014;431:31–41.
  153. Bae H, Ahmad T, Rhee I, Chang Y, Jin SU, Hong S. Carbon-coated iron oxide nanoparticles as contrast agents in magnetic resonance imaging. *Nanoscale Res Lett*. 2012;7:31–44.
  154. He W, Ai K, Lu L. Nanoparticulate X-ray CT contrast agents. *Sci China Chem*. 2015;58(5):753–60.
  155. Nazir S, Hussain T, Ayub A, Rashid U, MacRobert AJ. Nanomaterials in combating cancer: therapeutic applications and developments. *Nanomedicine*. 2014;10(1):19–34.
  156. Hu H-P, Chan H, Ujiie H, Bernards N, Fujino K, Irish JC, et al. Nanoparticle-based CT visualization of pulmonary vasculature for minimally-invasive thoracic surgery planning. *PLoS One*. 2019;14(1):e0209501.
  157. Ashton JR, Gottlin EB, Patz EF, West JL, Badea CT. A comparative analysis of EGFR-targeting antibodies for gold nanoparticle CT imaging of lung cancer. *PLoS One*. 2018;13(11):e0206950.
  158. Ghaghada K, Starosolski Z, Stupin I, Sarkar P, Annapragada A. Interrogation of evolving tumor vasculature using high-resolution CT imaging and a nanoparticle contrast agent. In: *Proceedings of the SPIE 10578, medical imaging 2018: biomedical applications in molecular, structural, and functional imaging, 105781C (2018)*. Houston: SPIE; 2018.
  159. Theerasilp M, Sungkarat W, Nasongkla N. Synthesis and characterization of SPIO-loaded PEG-b-PS micelles as contrast agent for long-term nanoparticle-based MRI phantom. *Bull Mater Sci*. 2018;41(2):42.
  160. Leftin A, Koutcher JA. Quantification of nanoparticle enhancement in polarized breast tumor macrophage deposits by spatial analysis of MRI and histological iron contrast using computer vision. *Contrast Media Mol Imaging*. 2018;2018:3526438.
  161. Curley SM, Castracane J, Bergkvist M, Cady NC. Functionalization and characterization of an MRI-capable, targeted nanoparticle platform for delivery to the brain. *MRS Adv*. 2018;3(50):3027–32.
  162. Hedgire S, Krebill C, Wojtkiewicz GR, Oliveira I, Ghoshhajra BB, Hoffmann U, et al. Ultrasmall superparamagnetic iron oxide

- nanoparticle uptake as noninvasive marker of aortic wall inflammation on MRI: proof of concept study. *Br J Radiol.* 2018;91(1092):20180461.
163. Jin SE, Jin HE, Hong SS. Targeted delivery system of nanobiomaterials in anticancer therapy: from cells to clinics. *Biomed Res Int.* 2014;2014:814208.
  164. Marie H, Lemaire L, Franconi F, Lajnef S, Frapart Y-M, Nicolas V, et al. Superparamagnetic liposomes for MRI monitoring and external magnetic field-induced selective targeting of malignant brain tumors. *Adv Funct Mater.* 2015;25(8):1258–69.
  165. Wang SH, Shi X, Van Antwerp M, Cao Z, Swanson SD, Bi X, et al. Dendrimer-functionalized iron oxide nanoparticles for specific targeting and imaging of cancer cells. *Adv Funct Mater.* 2007;17(16):3043–50.
  166. Tartaj P, Morales MDP, Veintemillas-Verdaguer S, Gonzalez-Carreño T, Serna CJ. The preparation of magnetic nanoparticles for applications in biomedicine. *J Phys D Appl Phys.* 2003;36(13):R182–97.
  167. Noriega-Luna B, Godínez LA, Rodríguez FJ, Rodríguez A, Larrea GZLD, Sosa-Ferreya CF, et al. Applications of dendrimers in drug delivery agents, diagnosis, therapy, and detection. *J Nanomater.* 2014;2014:19.
  168. Sangwan Y, Hooda T, Kumar H. Nanoemulsions: a pharmaceutical review. *Int J Pharma Prof Res.* 2014;5(2):1031–8.
  169. Mishra R, Son IG, Mishra R. A review article: on nanoemulsion. *World J Pharm Pharm Sci.* 2014;3:258–74.
  170. Anton N, Vandamme TF. Nano-emulsions and micro-emulsions: clarifications of the critical differences. *Pharm Res.* 2011;28(5):978–85.
  171. Vandamme TF, Anton N. Low-energy nanoemulsification to design veterinary controlled drug delivery devices. *Int J Nanomedicine.* 2010;5:867–73.
  172. Jaiswal M, Dudhe R, Sharma PK. Nanoemulsion: an advanced mode of drug delivery system. *3 Biotech.* 2015;5(2):123–7.
  173. Li X, Anton N, Zuber G, Zhao M, Messaddeq N, Hallouard F, et al. Iodinated alpha-tocopherol nano-emulsions as non-toxic contrast agents for preclinical X-ray imaging. *Biomaterials.* 2013;34(2):481–91.
  174. Attia MF, Anton N, Akasov R, Chiper M, Markvicheva E, Vandamme TF. Biodistribution and toxicity of X-ray iodinated contrast agent in nano-emulsions in function of their size. *Pharm Res.* 2016;33(3):603–14.
  175. Attia MF, Anton N, Chiper M, Akasov R, Anton H, Messaddeq N, et al. Biodistribution of X-ray iodinated contrast agent in nano-emulsions is controlled by the chemical nature of the oily core. *ACS Nano.* 2014;8(10):10537–50.
  176. Jarzyna PA, Skajaa T, Gianella A, Cormode DP, Samber DD, Dickson SD, et al. Iron oxide core oil-in-water emulsions as a multifunctional nanoparticle platform for tumor targeting and imaging. *Biomaterials.* 2009;30(36):6947–54.
  177. Mora-Huertas CE, Fessi H, Elaissari A. Polymer-based nanocapsules for drug delivery. *Int J Pharm.* 2010;385(1–2):113–42.
  178. Jhaveri AM, Torchilin VP. Multifunctional polymeric micelles for delivery of drugs and siRNA. *Front Pharmacol.* 2014;5:77.
  179. Trubetskoy VS. Polymeric micelles as carriers of diagnostic agents. *Adv Drug Deliv Rev.* 1999;37(1–3):81–8.
  180. Ganta S, Devalapally H, Shahiwala A, Amiji M. A review of stimuli-responsive nanocarriers for drug and gene delivery. *J Control Release.* 2008;126(3):187–204.
  181. Ward MA, Georgiou TK. Thermoresponsive polymers for biomedical applications. *Polymers.* 2011;3(3):1215–42.
  182. Cheng R, Meng F, Deng C, Klok HA, Zhong Z. Dual and multi-stimuli responsive polymeric nanoparticles for programmed site-specific drug delivery. *Biomaterials.* 2013;34(14):3647–57.
  183. Kong WH, Lee WJ, Cui ZY, Bae KH, Park TG, Kim JH, et al. Nanoparticulate carrier containing water-insoluble iodinated oil as a multifunctional contrast agent for computed tomography imaging. *Biomaterials.* 2007;28(36):5555–61.
  184. Soppimath KS, Aminabhavi TM, Kulkarni AR, Rudzinski WE. Biodegradable polymeric nanoparticles as drug delivery devices. *J Control Release.* 2001;70(1–2):1–20.
  185. Duncan R. The dawning era of polymer therapeutics. *Nat Rev Drug Discov.* 2003;2(5):347–60.
  186. Fuchs AV, Gemmill AC, Thurecht KJ. Utilising polymers to understand diseases: advanced molecular imaging agents. *Polym Chem.* 2015;6(6):868–80.
  187. Mahapatro A, Singh DK. Biodegradable nanoparticles are excellent vehicle for site directed *in-vivo* delivery of drugs and vaccines. *J Nanobiotechnology.* 2011;9:55.
  188. Reis CP, Neufeld RJ, Ribeiro AJ, Veiga F. Nanoencapsulation I. Methods for preparation of drug-loaded polymeric nanoparticles. *Nanomedicine.* 2006;2(1):8–21.
  189. Benzina A, Kruff MA, Bar F, van der Veen FH, Bastiaansen CW, Heijnen V, et al. Studies on a new radiopaque polymeric biomaterial. *Biomaterials.* 1994;15(14):1122–8.
  190. Mawad D, Mouaziz H, Penciu A, Mehier H, Fenet B, Fessi H, et al. Elaboration of radiopaque iodinated nanoparticles for in situ control of local drug delivery. *Biomaterials.* 2009;30(29):5667–74.
  191. Pimpha N, Chaleawlerlert-umpon S, Sunintaboon P. Core/shell polymethyl methacrylate/polyethyleneimine particles incorporating large amounts of iron oxide nanoparticles prepared by emulsifier-free emulsion polymerization. *Polymer.* 2012;53(10):2015–22.
  192. Galperin A, Margel S. Synthesis and characterization of radiopaque magnetic core-shell nanoparticles for X-ray imaging applications. *J Biomed Mater Res B Appl Biomater.* 2007;83(2):490–8.
  193. Kim D, Yu MK, Lee TS, Park JJ, Jeong YY, Jon S. Amphiphilic polymer-coated hybrid nanoparticles as CT/MRI dual contrast agents. *Nanotechnology.* 2011;22(15):155101.
  194. Kim D, Kim J, Jeong Y, Jon S. Antibiofouling polymer coated gold @ iron oxide nanoparticle (GION) as a dual contrast agent for CT and MRI. *Bull Kor Chem Soc.* 2009;30(8):1855–7.
  195. Skajaa T, Cormode DP, Falk E, Mulder WJ, Fisher EA, Fayad ZA. High-density lipoprotein-based contrast agents for multimodal imaging of atherosclerosis. *Arterioscler Thromb Vasc Biol.* 2010;30(2):169–76.
  196. Ng KK, Lovell JF, Zheng G. Lipoprotein-inspired nanoparticles for cancer theranostics. *Acc Chem Res.* 2011;44(10):1105–13.
  197. Allijn IE, Leong W, Tang J, Gianella A, Mieszawska AJ, Fay F, et al. Gold nanocrystal labeling allows low-density lipoprotein imaging from the subcellular to macroscopic level. *ACS Nano.* 2013;7(11):9761–70.
  198. Sabnis S, Sabnis NA, Raut S, Lacko AG. Superparamagnetic reconstituted high-density lipoprotein nanocarriers for magnetically guided drug delivery. *Int J Nanomedicine.* 2017;12:1453–64.
  199. Cormode DP, Skajaa T, van Schooneveld MM, Koole R, Jarzyna P, Lobatto ME, et al. Nanocrystal core high-density lipoproteins: a multimodality contrast agent platform. *Nano Lett.* 2008;8(11):3715–23.